CAPABILITY OF d^2 SPECTROMETRY FOR DETECTING RAMAN SCATTERING

By

WALLACE DORMAN KILPATRICK

A DISSERTATION PRESENTED TO THE GRADUATE COUNCIL OF
THE UNIVERSITY OF FLORIDA
IN PARTIAL FULFILLMENT OF THE REQUIREMENTS FOR THE
DEGREE OF DOCTOR OF PHILOSOPHY

UNIVERSITY OF FLORIDA

1975

ACKNOWLEDGMENTS

Acknowledgments are difficult to make because help has been offered in many ways, sometimes direct, sometimes unsolicited or casual. I am grateful for contributions from the University Librarians, the Department of Electrical Engineering, and the Department of Engineering Sciences, where this experimental work was done.

Without Dr. D. T. Williams, who is committee chairman, the subject investigation would never have been entered upon nor completed. His optimism, enthusiasm and confidence, and that of Dr. Knox Millsaps have been essential.

I would like to thank committee members Dr. T. L. Bailey, Dr. D. R. Keefer, and Dr. J. W. Dufty for several important discussions and genuine efforts. Specific contributions and motivations that have originated with Dr. G. D. Ward, Dr. A. A. Broyles, Dr. E. R. Chenette, Dr. A. H. Wing, and Dr. M. Zahn are deeply appreciated.

TABLE OF CONTENTS

	Page
ACKNOWLEDGMENTS	ii
LIST OF TABLES	iv
LIST OF FIGURES	v
ABSTRACT	vii
CHAPTER	
I INTRODUCTION	1
II GENERAL INSTRUMENTATION d^2 RAMAN SPECTROMETER	12
Optical Input	14
Modulator	16
Signal Channel	19
Synchronous Channel	24
Second Detector	27
III INSTRUMENT RESPONSE	30
Signal Intensity Calibrations	30
Tuned Amplifier	34
Random Noise and Interference	46
Interstage Decoupling	48
IV RESULTS AND DISCUSSION	50
Carbon Tetrachloride versus Toluene	58
Slit Modulation and Stability	70
Modified Sync Channel and Second Detector	72
V SUMMARY AND CONCLUSIONS	75
APPENDIX	
A WAVEFORMS OF SELECT POSITIONS IN ELECTRONIC CIRCUITS OF d^2 RAMAN SPECTROMETER	79
BIBLIOGRAPHY	86
BIOGRAPHICAL SKETCH	88

LIST OF TABLES

Table		Page
I	Features Appearing in Figure 14	52
II	Light Intensity in the Stokes and Anti-Stokes Regions of Figures 17 and 17 for Toluene	64
III	Light Intensity in the Stokes and Anti-Stokes Regions of Figures 18 and 19 for Carbon Tetrachloride	66
IV	Calculated Wavelengths Using Published Frequencies	69

LIST OF FIGURES

Figure		Page
1	Transmission function and profile coordinate scheme	7
2	Functional block diagram	13
3	Raman scattering cell	15
4	Modulator	17
5	Modulator	18
6	Quarter-meter monochromator	20
7	Signal channel	22
8	Synchronous channel	25
9	Second detector	28
10	Intensity calibration	32
11	Tuned amplifier characteristic	35
12	Equivalent network for tuned amplifier analysis	37
13	Tuned amplifier circuit model	42
14	Initial d^2 Raman spectrum of carbon tetrachloride	51
15	Typical d^2 line response	53
16	Toluene, Raman anti-Stokes spectrum	59
17	Toluene, Raman Stokes spectrum	60
18	Carbon tetrachloride, Raman anti-Stokes spectrum	61
19	Carbon tetrachloride, Raman Stokes spectrum	62

LIST OF FIGURES - Continued

Figure		Page
20	Amplitude of apparent lines on the Stokes and anti-Stokes sides of 6328 Å excitation for toluene	65
21	Amplitude of apparent lines on the Stokes and anti-Stokes sides of 6328 Å excitation for carbon tetrachloride	67
22	Raman Spectrometer, proposed option	73
23	Modulator, sensor amplifier output, U2	80
24	Master oscillator output, U1	80
25	Modulator, driver output to coil, Q4	81
26	Signal channel, preamplifier output, U5	81
27	Signal channel, tuned amplifier output, U7	82
28	Sync channel, square wave amplifier output, U3	83
29	Sync channel, doubler output, U4	83
30	Sync channel, doubler amplifier input, U4	84
31	Sync channel, doubler amplifier output, U6	85
32	Second detector, rectified tuned amplifier output, U8 input	85

Abstract of Dissertation Presented to the Graduate Council of the University of Florida in Partial Fulfillment of the Requirements for the Degree of Doctor of Philosophy

CAPABILITY OF d^2 SPECTROMETRY FOR DETECTING RAMAN SCATTERING

by

Wallace Dorman Kilpatrick

June, 1975

Chairman: Dr. D. T. Williams
Major Department: Aerospace Engineering

An outdated model d^2 Air Analyzer was used in this experimental investigation as a basis to estimate the capability of d^2 spectroscopy and to develop a d^2 Raman Spectrometer. The first d^2 Raman spectra, observed by Darling and Williams before this study, used a strong 800 milliwatt argon laser (4880 Å), which gave a signal-to-noise ratio, S/N $\cong$ 1. With extensive electronic modifications, the present investigation has resulted in a reduction of the noise to a level where Raman spectra using the same scattering cell are observed with a 3 milliwatt helium-neon laser (6328 Å) and S/N $\cong$ 1.

A d^2 Spectrometer is an instrument for direct, instantaneous recording of the second derivative of the profile of an optical spectrum line. It derives an especially high sensitivity from intensity modulation of the light transmitted through the spectrometer followed by amplification of only the second harmonic component of the photodetector. A phase-lock technique is then used to determine the cosine component

of this second harmonic, since the leading term of the cosine coefficient is proportional to the second derivative of the line profile.

Raman spectra are weak, scattered radiations, about 10^{-3} in relation to Rayleigh scattered radiations, where the Rayleigh radiation is 10^{-3} of the incident, precollision intensity. Raman lines appear only because some of the energy of the photon-molecule collision appears as internal molecular vibrational energy. The importance of the effect is that if the Raman lines can be measured, internal molecular structure can be inferred.

The modifications and tests show that the d^2 sensitivity limitation is due to electronic circuitry, and several background noise sources have been identified. Interstage coupling of operational amplifiers has involved different waveforms: square waves, fundamental and harmonic wobble frequencies, power supply ripple, beat frequencies, power line transients, parasitic oscillations, and the peculiar waveforms of regenerative and super-regenerative feedback. Because strong Raman signal levels appeared to be the order of 1 microvolt at the photodetector, the types of couplings and means to reduce their contributions below that level essentially outline the noise problem.

The means used to reduce noise levels have been: buffer isolation of each amplification stage from the power supply through the use of long time constant filters; isolation of each stage from the other by removing closed inductive loop

circuits and open capacitive circuits; stabilization (thermal, mechanical, and frequency) to minimize excursions; and reduction of the amplitude of all waveforms to minimum values consistent with reliable operation. A much quieter d^2 circuitry evolved, and further improvement appears possible.

At the present stage of development, observation of d^2 Raman spectra are marginal with a 3 milliwatt helium-neon laser and cylindrical Raman cell. Acceptable operation with S/N $\cong$ 100 for strong Raman lines could be obtained with various optional conditions: e.g., increase the helium-neon laser strength to 50 milliwatts with no other changes; or use at least a 10 milliwatt argon laser (4880 Å) because the frequency gives an increase of 2.83 in radiation and an increase of about 12 for photodetector sensitivity. Changes in Raman scattering cell efficiency cause linear scaling of any of these factors.

An optional d^2 circuit is presented where the lock-in feature and second harmonic detection are retained, but the "chopper" method of detecting the harmonic cosine coefficient is replaced by a quiet cosine analog system which integrates over the wobble frequency in a "Fourier coefficient" method. An innovative, quiet, all-electric modulator is also proposed which could be versatile in frequency adjustment, programmable for synchronous operation, and workable at a lower power level.

CHAPTER I

INTRODUCTION

This is an experimental investigation into the capability of d^2 instrumentation for detecting weak laser light scattered by the Raman effect. The d^2 principle of detecting optical signals was devised by D. T. Williams [1], developed by R. N. Hager, Jr. [2], and commercialized by the firms of Spectrometrics, Inc., Tampa, Florida [3], and Lear Siegler, Inc., Englewood, Colorado [4]. An outdated commercial Model III d^2 Air Analyzer, designed for monitoring the optical absorption of air pollutants, was modified and used as a basis for the high sensitivity instrumentation required for Raman spectroscopy.

Prior to this study, J. W. Darling [5] reported a laser Raman spectrum with the same Air Analyzer used here. Although he used a strong argon laser, 0.8 watts at 4880 Å, the resulting signal-to-noise ratio in the Raman spectrum was $S/N \cong 1$. Reasons for the poor performance of the d^2 instrumentation were presumably a "high noise level" of the instrumentation during operation. The observed "noise" was basically an erratic wandering of the base line (i.e., zero signal level) at a rate which was comparable to that of the scanned line signal. The Raman spectra were major lines of carbon tetrachloride and toluene, and appeared at known locations.

The instrumentation problem of sensitivity and noise can be appreciated from a relative scale of scattered light intensities, where the light may be scattered by small particles (Tyndall effect), whole molecules (Rayleigh effect), solids (Brillouin effect), or by individual atoms in molecules (Raman effect). Apparently the Rayleigh intensity, I_C, is about 10^{-3} that of the incident radiation [6]. Brillouin intensities, I_B, are less than Rayleigh intensities, I_B/I_C is about 10^{-1} for carbon tetrachloride and 10^{-2} for water; and Brillouin wavelength shifts are small. Raman intensities, I_R, are smaller yet, I_R/I_C is 10^{-3} or less [6] depending on the vibration levels of the energy absorbed. Raman frequency shifts, however, are greater than Brillouin shifts because modulation from atom-atom rotation, bending, and elongation frequencies are greater than for sound frequencies.

From simple theory of classical spectral emission, the amount of radiation depends on the frequency. Consider a steady, one-dimensional motion of a harmonically bound electron of charge e and mass m forced to vibrate by an external electromagnetic wave of amplitude E_o and frequency ν [7],

$$[d^2y/dt^2] + \nu'^2 y = [eE_o/m] \exp(j\nu t),$$

which has the solution

$$y = [eE_o/m][1/(\nu'^2 - \nu^2)] \exp(j\nu t)$$

In general, for $\nu' = 0$ the electron forms part of a dipole, p_o, which produces a radiation field E(r) at large r

and at angle θ from the dipole axis

$$E(r) = (\pi\, p_o\, \nu^2 \sin\theta/\varepsilon_o\, r\, c^2)\, \exp(j\nu t)$$

The radiated intensity varies as $E(r)^2$, so that after integration over all θ, the total intensity per unit time, I, has a classical fourth power frequency dependence

$$I = 4\,\pi^3\, p_o^2\, \nu^4/3\,\varepsilon_o\, c^3$$

where ε_o is the permittivity of free space, and c is the velocity of light. If the electrons are strongly bound, their motion is modified by the molecular motion of frequency ν' and the Raman intensity I_R is related to the incident intensity

$$I_R/I_C \sim (\nu'^2 - \nu^2)^2 \sim \nu^4 \qquad \nu' << \nu$$

Comparing the argon laser (4880 Å) data of Darling and Williams with that for a helium-neon laser (6328 Å), the Raman intensities would be less by at least a factor of $(4880/6328)^4 = 1/2.83$. Furthermore, scaling the power which they used (800 milliwatts) as well as the photomultiplier response, comparable results should be obtained with the 3 milliwatt helium-neon laser if the d^2 instrument sensitivity were improved by the factor $(800/3)(2.83)(12.5) = 9430$. The value 12.5 is the relative sensitivity of the particular photodetector used, obtained by the ratio of quantum efficiencies at 4880 and 6328 Å (10% and 0.8%, respectively).

Although complicated interpretations are necessary, the usefulness of Raman spectra are their value in inferring details of molecular structure. This usefulness, however, is tempered by the smallness of the effect. Modern Raman spectroscopy [8,9] employs, simultaneously, laser excitation to increase observable signal strengths, and a "double monochromator" to reduce background. Even for carefully designed monochromators, where careful attention is paid to internal baffling and minimal scattering, large amounts of stray radiation are always present. This radiation, as well as the desired Raman radiation, escapes through the exit slit. In double monochromators, the undesirable radiation is redispersed, reducing the interference. A good double monochromator presumably has a ratio of 10^{-9} between laser radiation transmitted at 10 cm^{-1}, and the line center [10]. In d^2 instrumentation, the stray radiation which escapes through the exit slit is identical, but modulated in time, and this modulation is in synchronism with the Raman line.

However, in the d^2 system, d^1 and d^0 are excluded from measurement. This means that the stray light is a noncontributor, unless it results from a virtual source correlated with the grating position in the manner of an optical "ghost." If such false lines should appear, then calibration of their location (i.e., laser transmission without Raman scattering present) identifies them, and the d^2 sensitivity to Raman spectroscopy is unimpaired. Therefore, the d^2

Spectrometer eliminates the need for a second monochromator function, rejecting background interference by electrical means.

A first requirement of the second derivative spectrometer is the equivalent of a "wobbler" in the form of an oscillating entrance slit to a single monochromator. The purpose of the wobble is to produce a time varying signal in the detector following the exit slit. The wobbler does this by moving periodically across the path of light emitted from the laser, and so causes the optical image at the output slit to move periodically across the output slit. When the optical line is centered at the exit slit, the wobble produces a second harmonic of the wobble frequency. When the line is not centered, a second harmonic still exists, its amplitude is less, and recurrent waveforms occur twice over each wobble period in a succession of even parity.

A second requirement for the d^2 spectroscopy is proper phase selection of the cosine component of the second harmonic. This is accomplished by rectification in phase-lock with the wobble frequency. In general, the phase of the detector signal varies with respect to the wobbler (modulating slit), and depends on the position of the spectrum lines at the detector. Accordingly, for a narrow slit which covers only a fraction of a line, only a phase increment is transmitted, and this has a particular phase relative to the steady state wobbler. In effect, a narrow slit scanning a line profile with the wobbler under fixed conditions produces an ac

signal with a phase proportional to the displacement. A forward wobble produces a signal which is followed by a similar (but reversed) pattern when the wobble reverses, thus giving a double frequency response. In general, phase-lock rectification (i.e., "chopping") produces positive or negative signals corresponding to positive or negative second derivatives of the spectrum line profile as the line is scanned.

To establish the relative importance between the phase and amplitude of the signal due to transmitted light, consider a mathematical convolution of a spectrum line profile with the exit slit width of 2b at x_o. Let the transmission function of the slit be rectangular, $T(x) = 1$, when $x_1 < x < x_2$, otherwise $T(x) = 0$. $x_2 = x_o + b$, and $x_1 = x_o - b$. See Figure 1 for the relation between these variables.

For a line with its maximum at x_o', not located at the center of the slit, x_o, the signal $S(x_o)$ which is transmitted through the slit to the photomultiplier is

$$S(x_o) = \int_{-\infty}^{\infty} I(x)\ T(x)\ dx$$

$$= \int_{x_1}^{x_2} I(x)\ dx$$

A Taylor expansion of $I(x)$ around x_o is convenient,

$$I(x, x_o) = I^{(0)}(x_o) + I^{(1)}(x_o)(x - x_o)$$

$$+ I^{(2)}(x_o)(x - x_o)^2/2! + \ldots$$

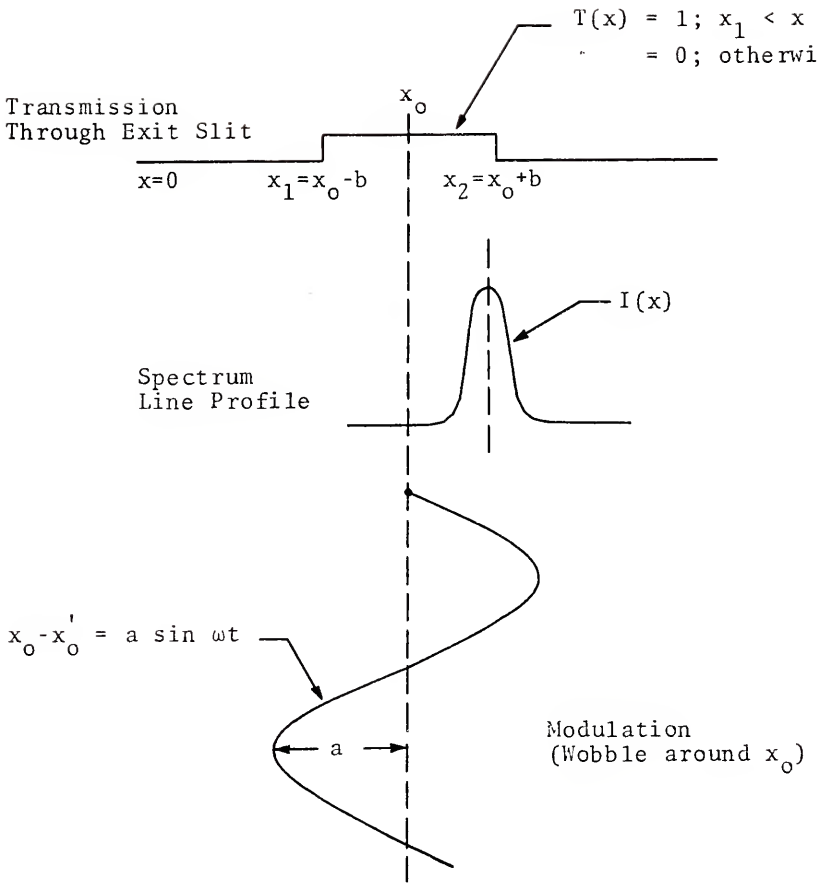

Figure 1. Transmission function and profile coordinate scheme.

where $I^{(n)}(x_o)$ is the n^{th} derivative of $I(x)$ evaluated at x_o. Integration over the limits gives

$$S(x_o) = I^{(0)}(x_o)[(x_2 - x_o) - (x_1 - x_o)]$$
$$+ I^{(1)}(x_o)[(x_2 - x_o)^2 - (x_1 - x_o)^2]/2!$$
$$+ I^{(2)}(x_o)[(x_2 - x_o)^3 - (x_1 - x_o)^3]/3! + \ldots$$

If the point $I(x_o)$ is periodically displaced by an amount a sin ωt, then the limits of integration, x_1 and x_2, are effectively

$$x_2 = x_o + a \sin \omega t + b$$

$$x_1 = x_o + a \sin \omega t - b \ .$$

The light signal transmitted is then

$$S(x_o) = A_o\, I^{(0)}(x_o) + A_1\, I^{(1)}(x_o)/2!$$
$$+ A_2\, I^{(2)}(x_o)/3! + \ldots$$

$$A_o = (a \sin \omega t + b) - (a \sin \omega t - b)$$

$$A_1 = (a \sin \omega t + b)^2 - (a \sin \omega t - b)^2$$

$$\vdots$$

Terms of the form $\sin^n \omega t$ can be expressed as multiple frequencies of the wobble frequency with the use of the

relation

$$\sin^{2n}\omega t = (1/2^n)(1 - \cos 2\omega t)^n \ .$$

To minimize the mathematical manipulations, and before substituting for $\sin^n\omega t$, recall that the d^2 instrument has a capacitor following the photomultiplier so that no dc signal levels are admitted, and it also has a tuned amplifier which responds to the second harmonic of the wobble frequency. If the mathematical operation E_h is defined as the selection of only the even second harmonics terms, i.e., excluding constant terms (dc), excluding odd harmonics (sines), and excluding all other frequencies, then the following terms appear for S(x):

$$E_h \cdot A_o = E_h\ (2b) = 0$$

$$E_h \cdot A_1 = E_h\ (4ab \sin\omega t) = 0$$

$$E_h \cdot A_2 = E_h\ (6a^2b \sin^2\omega t + 2b^3) = [-3a^2b] \cos 2\omega t$$

$$E_h \cdot A_3 = E_h\ (8a^3b \sin^3\omega t + 8ab^3 \sin\omega t) = 0$$

$$E_h \cdot A_4 = E_h\ (10a^4b \sin^4\omega t + 20\ a^2b^3 \sin^2\omega t + 2b^5)$$
$$= [-5a^4b - 10a^2b^3] \cos 2\omega t$$

$$E_h \cdot A_5 = E_h\ (12a^5b \sin^5\omega t + 40a^3b^3 \sin^3\omega t + 12ab^5 \sin\omega t)$$
$$= 0$$

$$E_h \cdot A_6 = E_h\ (14a^6b \sin^5\omega t + 70a^4b^3 \sin^4\omega t + 42a^2b^5 \sin^2\omega t$$
$$+ 2b^7) = [-7a^6b - 35a^4b^3 - 21a^2b^5] \cos 2\omega t$$

. . . .

The first d^2 instrument terms of the photomultiplier signal are then

$$E_h \cdot S(\omega t) = -a^2 b[I^{(2)}(x_o)/2! + I^{(4)}(x_o)/4! \cdot (a^2 + 2b^2) + I^{(6)}(x_o)/6! \cdot (a^4 + 5a^2b^2 + 3b^4) + \ldots] \cos 2\omega t \, .$$

This result does not agree precisely with that of Hager [9], because the development and analysis are different. Here the intensity distribution is integrated over the slit width before the time variation is introduced. However, for a specific profile (i.e., sin x/x), Hager finds that the leading term of $I^{(2)}(x_o)$ for the second harmonic is proportional to a^2, which is an order of agreement. Otherwise, there is no statement for comparison.

In general, extracting the second harmonic with a filter mechanism, and selecting only the cosine component with a phase-lock mechanism, results in an effective approximation to the second derivative of the arbitrary profile function, I(x). The mathematics indicates that only even order derivatives are observed. Amplitudes decrease with order, and an oversimplified measure of importance of terms is indicated by the ratio of d^2 to d^4 which, for an assumed Gaussian profile, would be 6:1 at the center of the line.

To complete a description of second derivative instrumentation, it is necessary to provide for the line to be scanned in order to correlate the observed intensity with

$d^2(I(x))$ whenever the line crosses the exit slit. A simple technique of recording in synchronism with the moving grating provides such a d^2 profile of a line.

It is important to note that Fresnel diffraction patterns are not considered here because the image of the first slit is produced by optical focusing at the second slit while the Fresnel patterns incident on the grating, for example, are subsequently focused into a "line." Also, Fresnel patterns after the second slit occur over the detector surface where all of the light from the second slit is collected, and therefore the electrical output is not altered.

Because noise (i.e., erratic zero-signal level) seemed at the time to be the major limitation in laser d^2 Raman spectroscopy, the present investigation was designed to examine practical noise sources and to eliminate unstable electronic performance. The Model III Air Analyzer was used as a starting point, and extensive modifications which evolved are described below. The cataloging of Raman lines, derivations of molecular structures from Raman line information, and research into laser properties -- all of which have bearing on d^2 performance -- have been essentially avoided because they are extensive subject areas in their own right.

CHAPTER II

GENERAL INSTRUMENTATION d^2 RAMAN SPECTROMETER

Raman d^2 instrumentation consists of the functional parts: optical input, modulator (wobble generator), signal channel, synchronous (sync) channel, second detector and recorder output, as shown in Figure 2. Except for the Raman scattering cell and laser, d^2 instrumentation is the foundation of the system.

Extensive modification of a d^2 Air Analyzer resulted in such improved d^2 sensitivity that Raman spectra of carbon tetrachloride were detected with a He-Ne laser of 3 milliwatts. The main limitation for Raman d^2 spectroscopy has turned out to be not the d^2 principle, or light scattered in the spectrometer, but various electronic couplings in the form of cross-talk between components. In particular, printed circuits were used, a construction which offered means (but not the only means) for undesirable interstage coupling. Accordingly, observation of Raman spectra, after accomplishing some degree of isolation between electronic components and their functions, indicates that even greater sensitivity using the d^2 principle is possible. Redesign with hard wiring and with special attention to electrical decoupling techniques should produce either or both an advance in the state-of-the-art for Raman

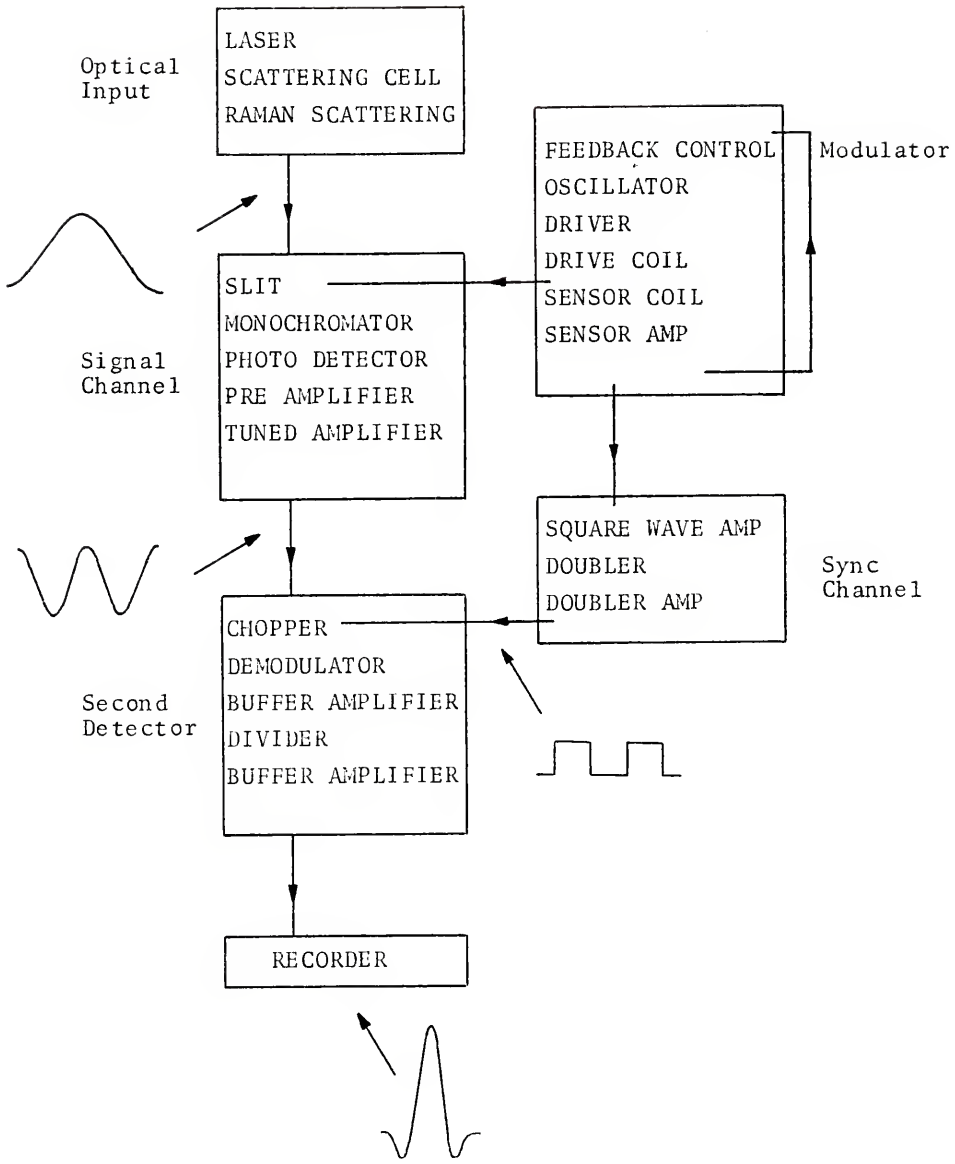

Figure 2. Functional block diagram.

spectroscopy (sensitivity), or a considerable reduction in cost for performance comparable to that of a double monochromator.

The arrangement and circuitry described below is not an ultimate, but rather the specific system in use when the 3 milliwatt He-Ne Raman d^2 spectrum of carbon tetrachloride was observed. Additional specific changes have been made, but the principles are the most important to record, because redesign alone is insufficient to avoid relocating some of the sources of undesirable noise, instability or crosstalk.

Optical Input

Optical input is derived from a 3 milliwatt He-Ne laser, Model 132, made by Spectra Physics [11]. The laser emission enters a cell, as shown in Figure 3, which was used by Darling and Williams for detecting Raman scattering from liquids. The glass cell has aluminum vacuum-evaporated on the exterior surfaces and acts as a multiple-reflecting surface to increase the effective path length of the laser radiation through the sample liquid. A void of 1 mm by 5 mm in the vacuum coating allows the laser energy into the cell. Although this is neither a sophisticated nor efficient Raman scattering cell, it serves the purpose of evaluating d^2 Raman spectroscopy.

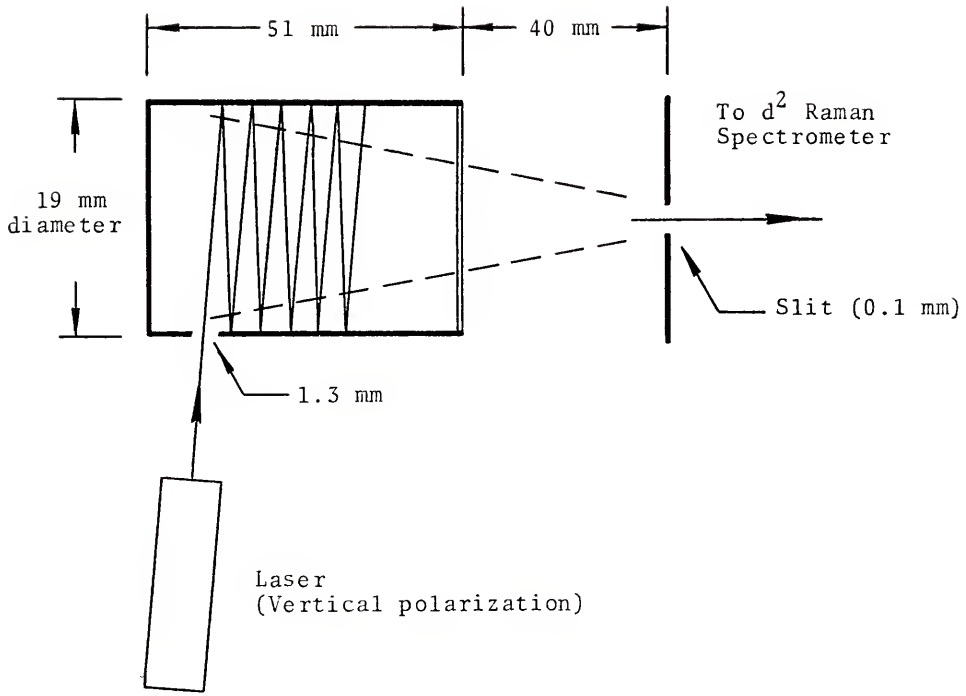

Figure 3. Raman scattering cell.

Modulator

The starting point of the modulator is the vibrating entrance slit of the monochromator. The slit moves physically on the order of a slit width, 0.1 mm, across the optical path of light emitted from the Raman scattering cell. This causes an intensity modulated signal to pass through the monochromater to the photodetector. Accurate control of the slit vibration is critical.

A driver coil and a sensor coil are attached to the slit, and both of these coils are electrically included in a feedback loop with a free-running oscillator. The object of the feedback loop (collectively this is the modulator shown in Figures 4 and 5, and wobbles the slit) is to maintain constant slit oscillatory amplitudes by varying the oscillator drive power. The oscillator frequency is about the same as the natural mechanical frequency of the slit assembly, nominally 45 Hz.

Both frequency and amplitude stability are essential for d^2 Raman spectroscopy because of the necessary averaging of the rectified second harmonic component of the optical signal. For example, each line scan occurs over a finite time interval so that variation in the integration limits of the rectified signal equates with amplitude variation. Measured variation in the modulation frequency was less than one period in 10 min, i.e., one part in 2.7×10^4.

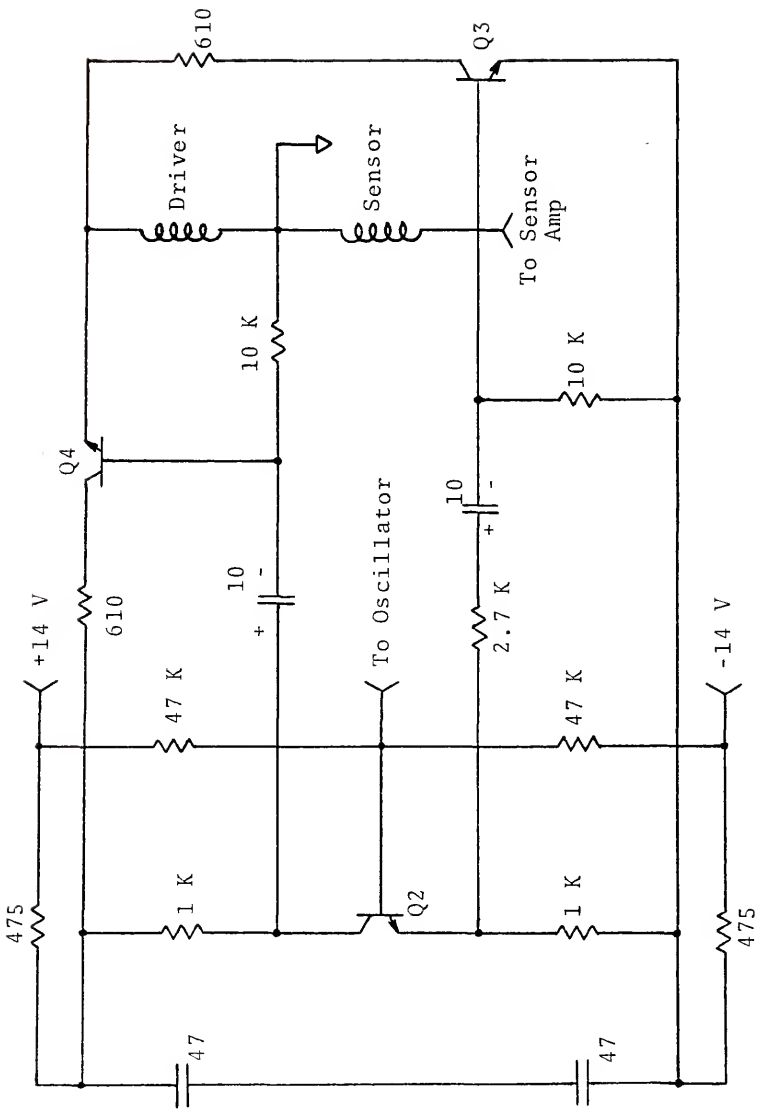

Figure 4. Modulator (drawing 1 of 2).

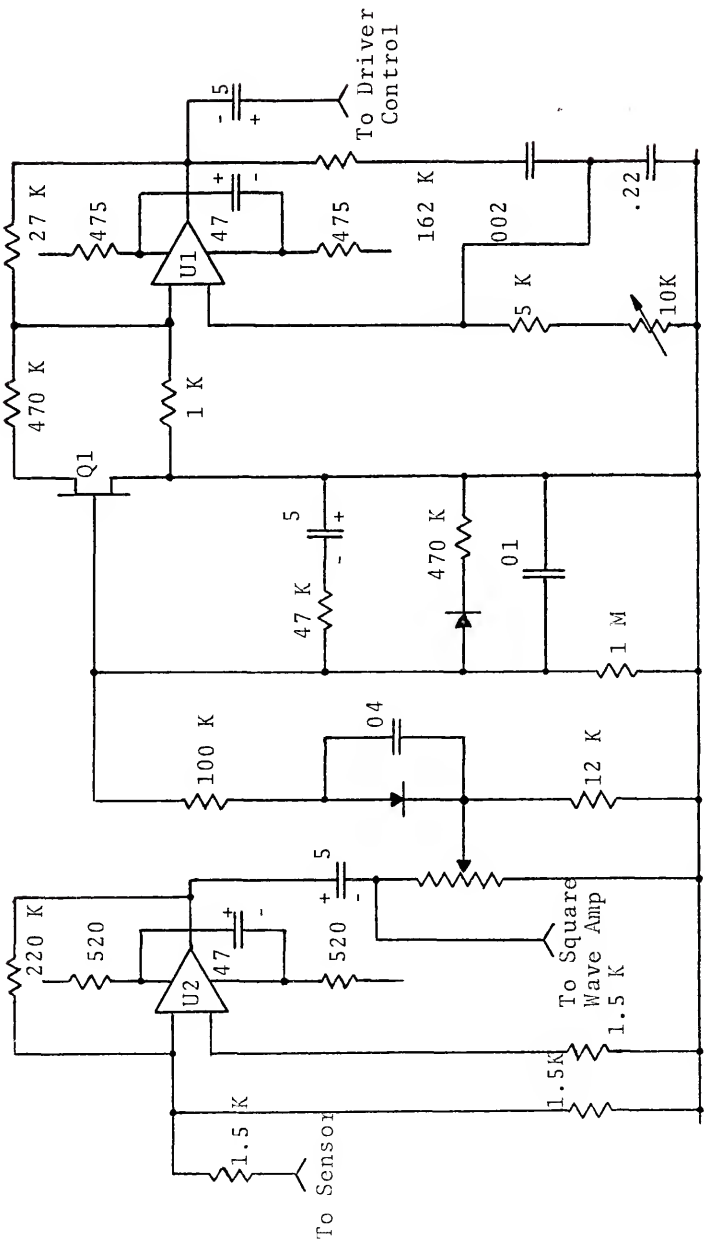

Figure 5. Modulator (drawing 2 of 2).

The sensor coil output is a sinusoidal voltage, derived from sinusoidal slit motion carrying the sensor coil through a local magnetic field. The sensor amplifier, U2, inverts the signal which is then rectified to obtain a negative bias with a long decay time of several seconds (5 μf x 1 M = 5 sec). This negative bias regulates the input of a field effect transistor whose output in turn adjusts the bias of the electronic oscillator U1. The power output of U1 is thus reduced if the sensor voltage is excessive (large oscillation amplitude). A 10 K potentiometer in the common leg adjusts the frequency of U1 by changing the time constant of its feedback.

Signal Channel

Raman scattered light which is transmitted through the entrance slit goes through a quarter-meter Ebert monochromator, Model 82-410, manufactured by Jarrel-Ash [12]. Details of the monochromator arrangement are shown in Figure 6. Optical transmission through the monochromator occurs if a diffuse light source is placed before the slit but within an angle defined by the mirror diameter to focal length, 38/250, or about ±5 degrees around the optical axis. Omnidirectional Raman scattering originating in this region is accepted for transmission, so that for a given laser excitation, normal to the slit and to the optical axis, the amount of Raman radiation reaching the slit is constant provided the sample and the excitation fill the acceptance region. Since the entrance

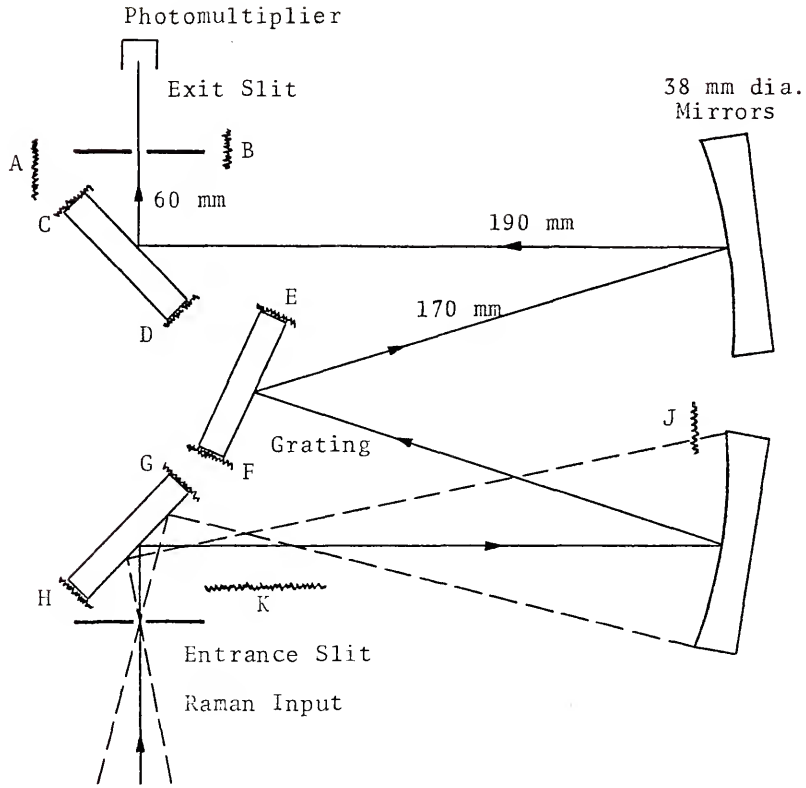

Speed: f6.5.

Grating: Dispersion = 33 Å/mm, 11,000 lines/mm,
Blaze at 5000 Å, Plane and 64 mm x 64 mm.

Modifications: Baffling at B,J; Felt at A,K;
Opaque paint at A,C,D,E,F,G,H.

Figure 6. Quarter-meter monochromator.

slit causes a Fresnel pattern to appear across the mirror and grating surfaces, more intense lasers cause more intense patterns, which in turn cause more stray radiation backgrounds. Attenuation of the stray radiation is accomplished by addition of baffles and absorption materials.

The grating is a replica, made from the "sandwich type" construction where the master (typically ruled Au or Al) is coated with separation oil, then aluminum is vacuum-deposited on it, and a sandwich is formed when the entire assemblage is epoxy-glued to a glass base. The replica surface is then formed when the master and oil are removed. It is not uncommon to find spurious light penetration into the thinner parts of the groove structure, but it has been observed here only under direct illumination with the 3 milliwatt helium-neon laser and did not jeopardize its use for Raman spectroscopy.

The electrical part of the signal channel consists of a photomultiplier, a preamplifier and an amplifier tuned to double the wobble frequency, as shown in Figure 7. The photomultiplier output is negative, showing short negative noise pulses of about 10 μseconds' duration and 1 μvolt amplitude. Groups of pulses form into a negative waveshape in synchronism with the motion of a spectrum line as it crosses the exit slit. Two waveshapes are generated for each wobble, and these waveshapes "fuse" together when the center of the spectrum line appears at one end or the other of the slit. Thus a "phase effect" appears in the photomultiplier waveshape, and continues into the following tuned amplifier.

The photodetector is a seven-stage photomultiplier, Model 9783B, made by EMI [13], and operated from an 800-volt battery which is by-passed with 0.125 μf. This photomultiplier has a characteristic quantum efficiency of 15, 17, 10, and 2% at 2000, 3500, 4880, and 6000 Å, respectively. At 6800 Å the efficiency is 0.1%, essentially zero. The noise level according to the manufacturer is about 0.1 na of average dark current. The observed peaks of 1 μv across 100 K are 0.01 na, which generally agrees because of 10% on-time. The d^2 instrumentation handles the noise output easily, but not the low signal response at 6328 Å (1% quantum efficiency). A quantum efficiency of 15%, factor of 15 increase in sensitivity at 6328 Å, can be obtained with a more expensive end-on linear photomultiplier, Model 9658B, from the same manufacturer.

The preamplifier input is also the photomultiplier load, but the circuit frequency response can be low, 45 Hz. An important point in the preamplifier design is to discourage high frequency amplifications and also regenerative feedbacks, because they are both sources of unstable operation. To accomplish this, a 0.01 μf capacitor is placed between the output and input terminals of the amplifier U5, and a 14 K resistor is put in series with the input to decouple feedback through the printed circuit from the following tuned amplifier stage. In fact, without these decoupling means, a "super-regenerative" action of the preamplifier occurs when a signal results from any convenient transient and quenches itself in such a

way as to contribute false signals which are completely unacceptable for Raman spectroscopy. The frequency response of the preamplifier prior to degenerative feedback was broadly peaked at about 10 KHz, which became the characteristic frequency of the "super-regenerative" action. Super-regenerative action is not necessarily undesirable, since it exploits the high gain which appears near resonance, but practically it is unstable and a source of considerable noise.

The tuned amplifier is a double-tee filter connected as an active amplifier. It has a gain of about 500 at twice the wobble frequency, a bandwidth of about 12 Hz, and an exceptional stability. It seems to respond to harmonics, but it works well in the signal channel. It is a very interesting device and its performance will be pursued further.

Synchronous Channel

The purpose of the synchronous channel (sync channel), which is represented in Figure 8, is to provide the proper phase for rectifying (chopping) the tuned amplifier signal. Phasing is referred to the sensor coil, actually the sensor amplifier, so that changes in wobble frequency do not influence the phase relation between the signal channel and the chopper. The sync channel consists of a square wave amplifier, doubler, and doubler amplifier. It is important that the sync channel introduce no jitter or unstable operations, because changes in the chopper limits influence the time

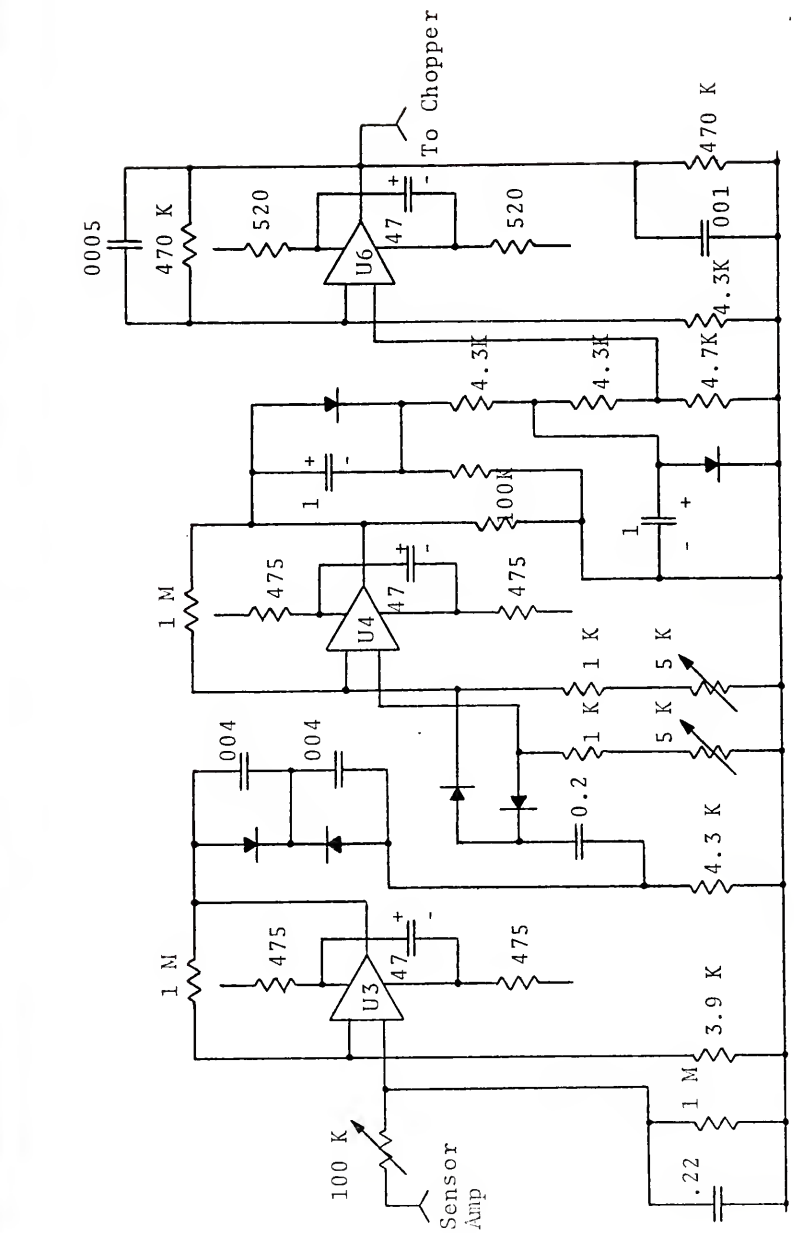

Figure 8. Synchronous channel.

constant integrator as effectively as variations in optical signal strength.

The square wave amplifier, U3, converts a sinusoidal input into a square wave by driving the input in excess of its linear limits. Two zener diodes in the output increase the rate of rise of the leading and trailing edges of the square wave, but shunting capacitors are provided to reduce jitter as the waveform crosses the zero potential level. Small phase adjustments are possible with the 100 K potentiometer input.

The doubler consists of two "peaker" RC elements which effectively differentiate each edge of the square wave, thus doubling the basic frequency. Adjustment of the resistive elements is provided for balancing on and off conduction times, so that equal duration pulses can be set. The trailing edge of each "peak" has inherently less rate of change in its decay, and can be a source of jitter in the operation of the integrated circuit amplifier, U4. Practically, the variations are typically 5 microseconds which, over a half period of 11 milliseconds, represents a variation of 5 parts in 10^4.

Output from the doubler can cause ringing, a parasitic behavior, in the following doubler amplifier stage, U6. The ringing is reduced by changing the waveform to a softer, sinusoidal shape by introducing 1 μf shunts across the zener diodes in the U4 output. Further suppression of ringing is accomplished by adding an 0.0005 μf capacitor across the feedback resistor of the doubler amplifier, as well as 0.001 μf

across its output resistor. A sharp switching of the chopper function is less important than consistent stable operation.

Second Detector

The second detector is a group of functions, as shown in Figure 9, which starts with a second harmonic of the wobble frequency of amplitude proportional to the optical signal, and ends up with a dc signal proportional to the same optical signal. Inputs from both the signal channel and the sync channel are required for a dc output to the recorder.

The second harmonic output from the tuned amplifier is rectified by proper timing (i.e., proper phase with respect to the wobble) of the conductance of a field effect transistor, Q5. This rectified signal, which may be either positive or negative depending on the optical signal phase, is then integrated (demodulated) to essentially a dc level by a time constant circuit of 100 seconds (500 μf x 200 K) before entering the buffer amplifier, U8. At this point, dc signals are relatively small.

The analog device AD/426 is a transconductance type divider, in a mathematical sense. Two input voltages, Z and X, when properly connected, result in an output Y, where Y = Z/X. In the present description of a d^2 Raman Spectrometer, the AD/426 device is used as a variable dc amplifier, controlled for convenience by the dc level, X, derived from a 1.5-volt, size AA battery. The divider was originally used

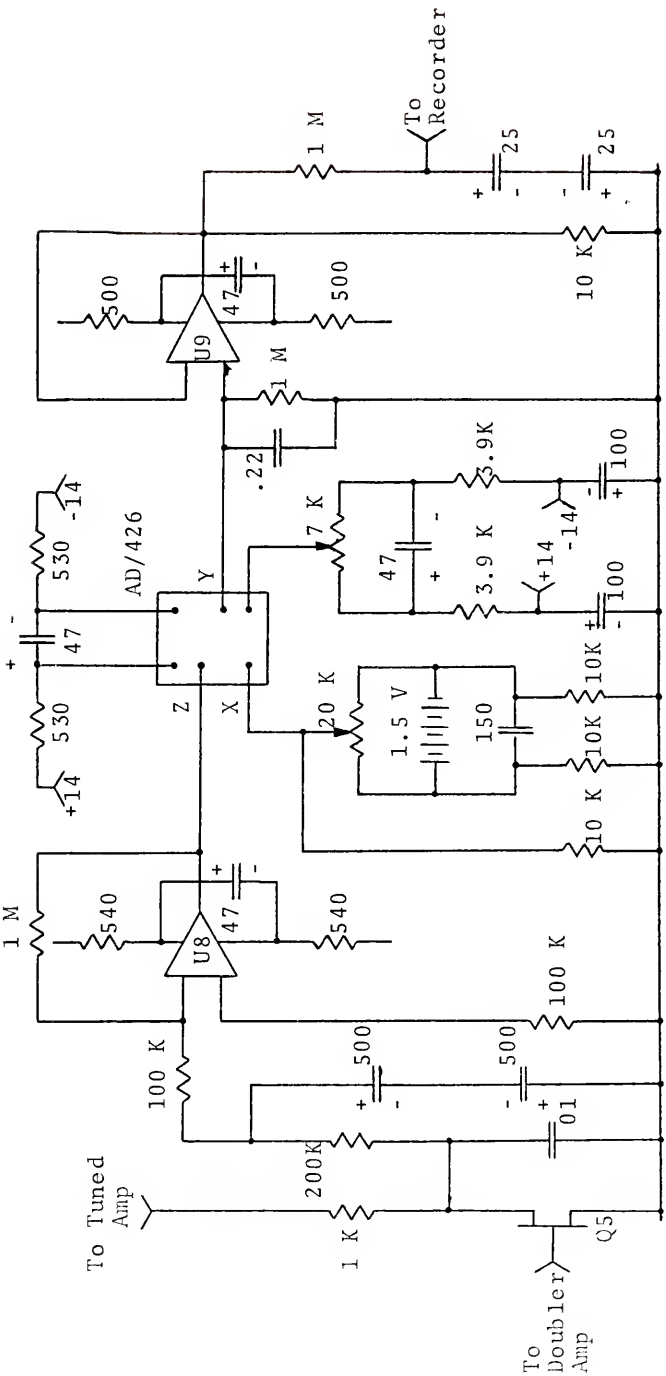

Figure 9. Second detector.

in the Air Analyzer absorption spectrometer as a normalizing device, in the mathematical sense, to compensate for changes in light source intensity -- a d^0 function. This feature is not useful for Raman d^2 spectroscopy where maximum sensitivity is always desired.*

The final stage of the second detector is a buffer for isolating the AD/426 device and the recorder. A long time constant of 25 seconds is introduced into the output to aid in the integration of noise which may have appeared after the rectifier time constant of 10 seconds. The total time response of the dc section is the result of these two time constants, practically about 30 seconds.

---

*A good description of a transconductance multiplier/divider can be found in reference 14. It is basically a thermally well-balanced operational amplifier which contains an additional control terminal to the usual operational amplifier. The output current is proportional to the voltage at its input terminals; output current, I_o, is the product of mutual conductance, g_m, and applied voltage, X, $I_o = g_m X$. When $g_m \approx Y$, then $I_o \sim X \cdot Y$, an analog multiplication function.

CHAPTER III

INSTRUMENT RESPONSE

The d^2 Raman Spectrometer has optical, electronic and mechanical features to consider, but the chief innovative advantage for Raman spectroscopy comes through the electronics treatment of the light signal and background noise. Since the Raman scattering intensity is about 10^{-6} that of the incident light, a known optical sensitivity of the system should indicate the laser excitation intensity, I, required to produce usable signals. If the electronic noise level could also be established at the same time, then the d^2 performance should be predictable.

Signal Intensity Calibrations

If the helium-neon laser (6328 Å) of 3 milliwatts is aimed directly into the acceptance cone of the modulating slit, there will be a major one-line contribution to the photomultiplier. Attenuation of the radiation by absorbers or scatterers will then allow extrapolation to laser intensity (upper limit) and noise levels (lower limit). Between these extremes is the dynamical range of the system where the Rayleigh and Raman spectra should fall to be useful.

Three- by five-inch index cards turned out to be very uniform in quality, and when clipped together to form a minimal spacing between the cards, made a convenient reproducible variable strength scatterer. The scattering stack apparently followed Lambert's law where the ratio of intensity leaving the stack to that which enters is a constant per card. Assuming that intensity, I, is diminished to a value I_k after passing through k cards, and that the decrease is proportional to the number of cards,

$$dI_k/dk = -\alpha I_k \ , \qquad \alpha = \text{constant}$$

$$I_k = I_o \, e^{-\alpha k} \ .$$

Thus, the intensity recorded by the d^2 system should be semi-logarithmic versus the number of cards. This relationship was consistent with signals which were electrically attenuated, and for each of the intensity levels over the measured range.

Measurements of intensity are displayed in Figure 10 as $\log_{10} F \sim$ number of attenuating cards, k, in the scattering deck. F is an intensity index, the product of recorder amplitude, electrical attenuation, and divider voltage (analog device AD/426 [15]) -- all in arbitrary units -- taken when the stack was located 60 mm from the slit between the slit and the laser.

The slope of a line through experimental points gives an absorption constant of $\alpha = 0.95$, and represents an average output to input factor of $e^{0.95} = 2.58$ per card. Extrapolation to zero cards gives an intercept of 2.2×10^4. The

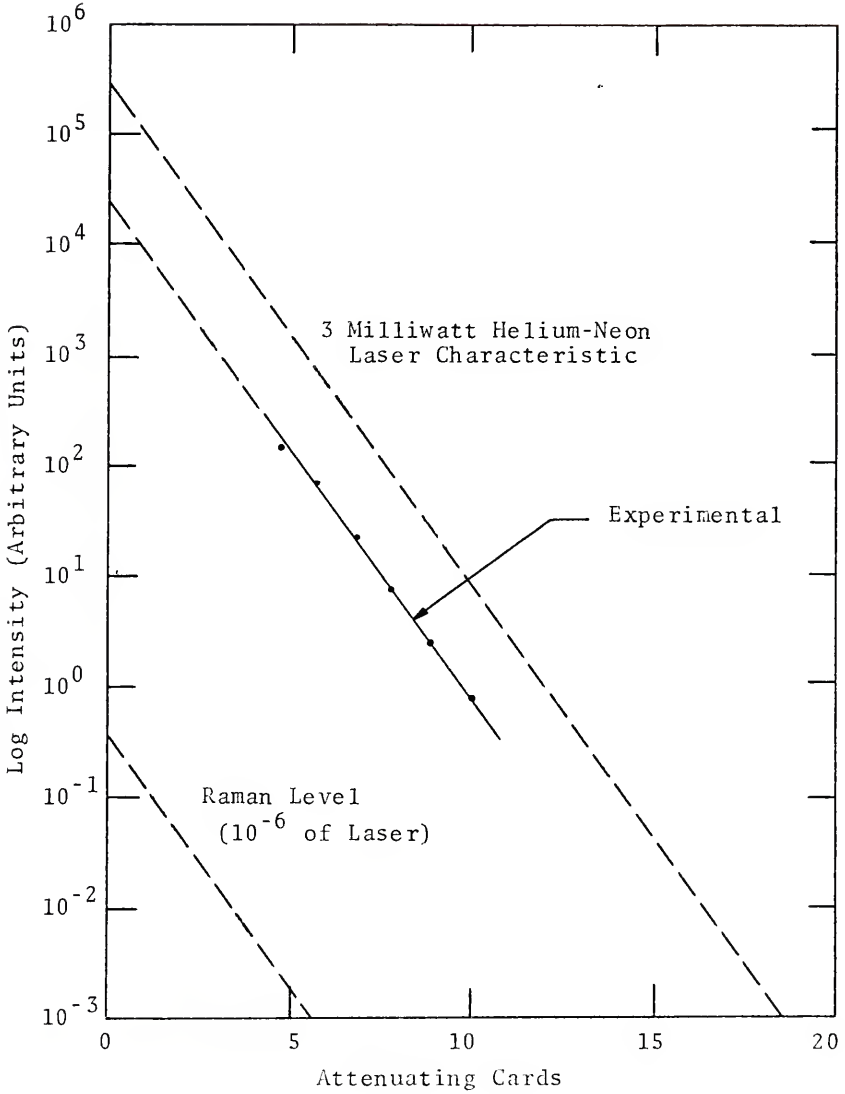

Figure 10. Intensity calibration.

available excitation for Raman spectra, however, is a little more than this, because the laser diameter of 1 mm covers more than the slit width of 0.1 mm. A characteristic laser line then, corrected for this overlap, would have an intercept at 2.2×10^5, up by a factor of 10, but with the same slope as the experimental curve.

If the recorder noise level were a fraction, 10^{-6} that of a fictitious recorder level due to total laser input, then typical Raman radiation would appear at $F = 2.2 \times 10^{-1}$ with $S/N \cong 1$. This assumes complete utilization of the excitation radiation and no Raman energy loss between the scatterer and the d^2 signal channel.

Experimental results are in reasonable agreement with this analysis. During the Raman spectrum run with carbon tetrachloride, for example, there was a noise level of $F = 3 \times 10^{-2}$, which should have given $S/N = (2.2 \times 10^{-1})/(3 \times 10^{-2}) = 7.3$. The observed S/N was about 4, which appears to be a very good agreement. But the agreement simply ignores losses from multiple laser reflections in the scattering cell, losses which are due to the optical acceptance angle at the entrance slit, and losses due to the angular distribution of the Raman radiation.

The helium-neon laser also has a spectrum of neon lines of low intensity associated with the conventional gas discharge, and Rayleigh scattering from these relatively weak lines can compete with the Raman scattering from the stimulated laser line. An estimate of their strength can be

obtained by applying the absorber method of intensity calibrations. Experimentally, the factor F is about 10^{-1} for many neon lines in this particular laser, so that without an optical filter, the Raman lines must be differentially picked out from the Rayleigh neon background. This also means that the ratio of laser light to a typical neon background line is about $2.2 \times 10^{4}/10^{-1} \approx 2 \times 10^{5}$.

Tuned Amplifier

The tuned amplifier is required to be sensitive only to the second harmonic of the modulated light signal. The degree to which d^0 and d^1 signals are rejected at the tuned amplifier is thus critical for d^2 performance. Experimental characteristics of the tuned amplifier are shown in Figure 11. where the tuned amplifier was effectively isolated, excited by a test sinusoid oscillator, and the output measured with an oscilloscope. The insert circuit diagram shows a test resistance, R", added as a parameter for evaluating the detuning effect as the Q of the circuit becomes modified. Otherwise, circuit constants are those used in U7 of Figure 7. Experimentally, the center frequency for R" = 0 is 86.2 Hz compared with the 60 Hz power line frequency.

The tuned amplifier has a double feedback mechanism, a so-called "double-T" filter, as pointed out earlier, and shown in Figure 11. A patent for this double T-network was granted to Augustadt [16] in 1938, and the first literature description

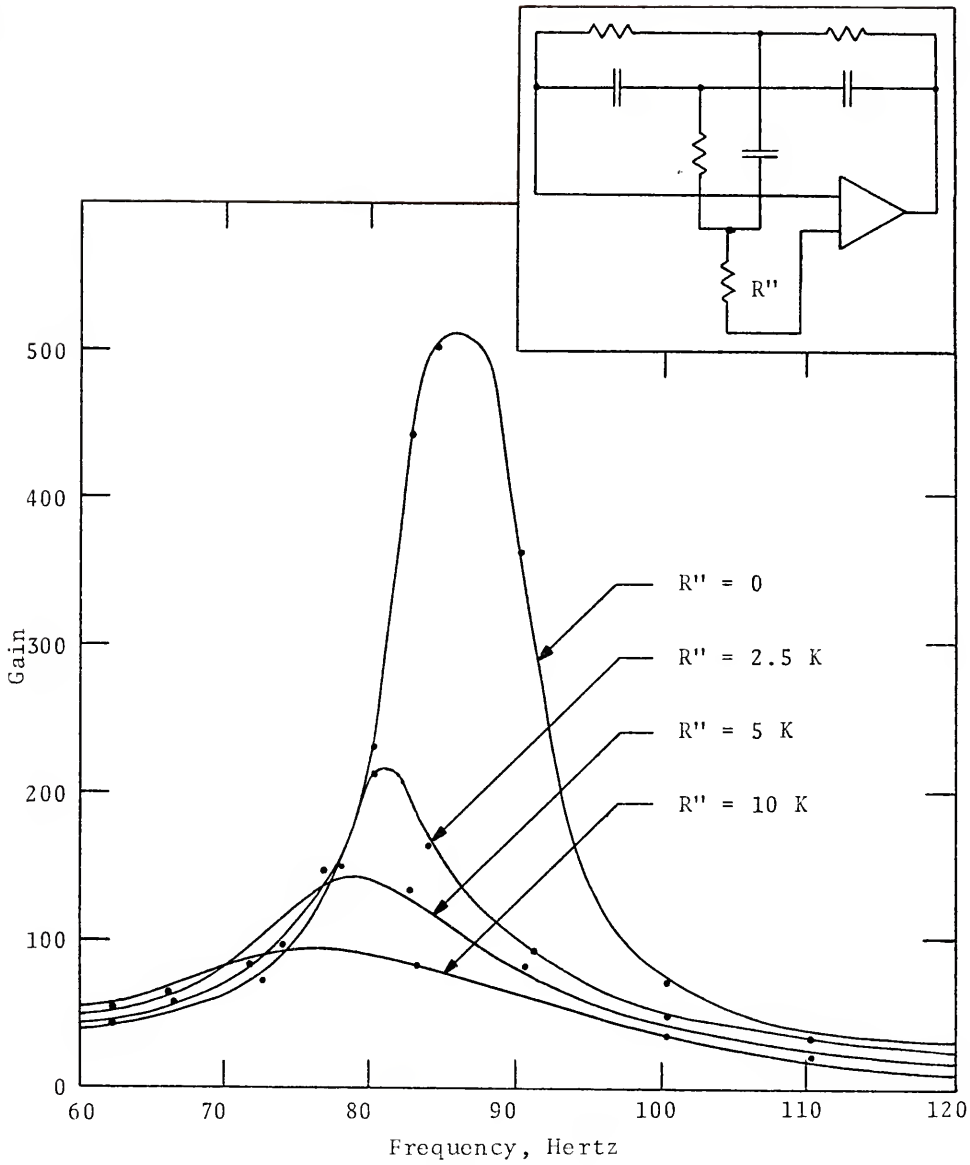

Figure 11. Tuned amplifier characteristic.

was given by Scott [17], also in 1938. The device has been subsequently developed and miniaturized [18-21], but with apparently limited applications, perhaps because it is most effective at very low frequencies which are seldom used.

The objective of the following analysis is to develop a mathematical model for the observed frequency response of the tuned amplifier, and the purpose is to acquire perspective for application of these data to the instrumentation. Two steps are required for a simple model -- first, the reduction of the double T-network to an equivalent double Π-network; and second, the formation of an amplifier circuit which uses the equivalent network [22].

To develop an equivalent Π-network, consider an approach similar to that of Stanton [18]. In steps of evolution, a single T-network, Figure 12(a), can be expressed as a single Π-network, Figure 12(b). Then two equivalent Π-networks can be arranged as a double Π-network, Figure 12(c), and finally the double Π-network can be arranged as a single Π-network which has terminal impedances which are identical with the original double T-network.

The general relation for the T-network to Π-network conversion is well known and easily derived [23]. The result is

$$Z_A Z_2 = Z_B Z_3 = Z_C Z_1 = H \ ,$$

where H is defined for convenience as the function

$$H = Z_1 Z_2 + Z_1 Z_3 + Z_2 Z_3 \ .$$

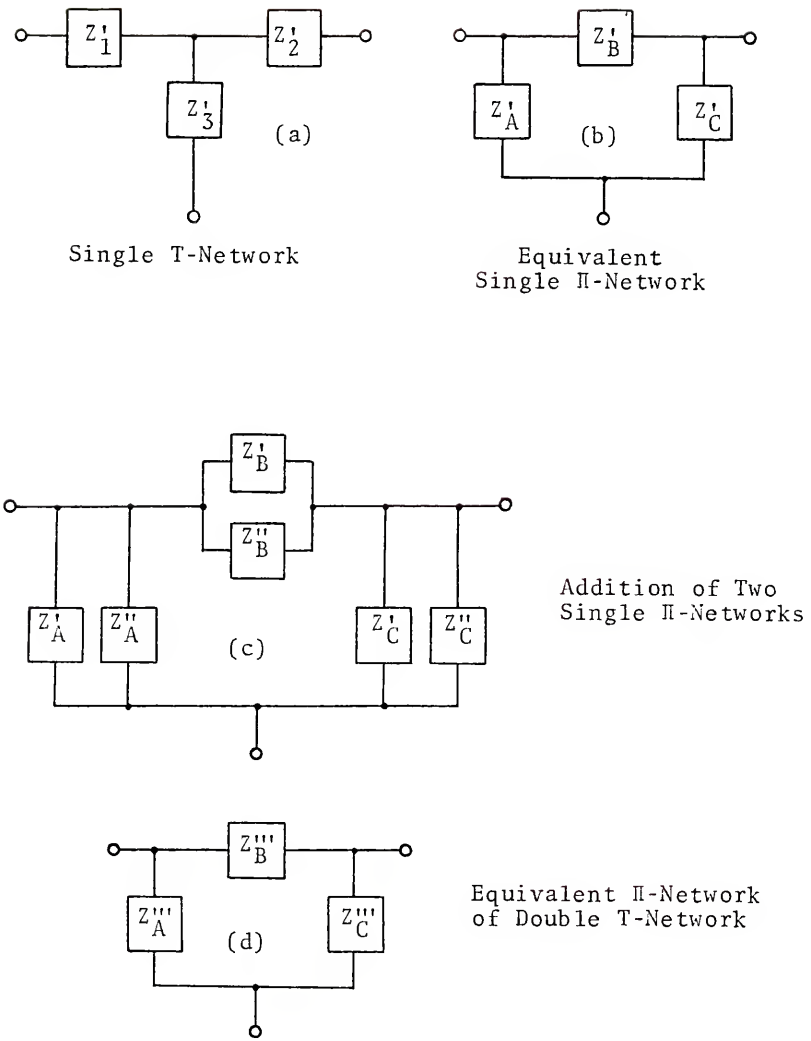

Figure 12. Equivalent network for tuned amplifier analysis.

For one branch (primed quantities) and the other branch (double primed quantities), the composite equivalent Π-network (triple primed quantities) components are

$$Z'''_A = Z'_A Z''_A/(Z'_A + Z''_A)$$

$$Z'''_B = Z'_B Z''_B/(Z'_B + Z''_B)$$

$$Z'''_C = Z'_C Z''_C/(Z'_C + Z''_C) \ .$$

To find the frequency where there is maximum gain, the feedback must be zero -- either Z'''_A vanishes, or Z'''_B becomes infinite at some particular frequency. The first case is denied because of the finite resistance of elements in the circuit. However, Z'''_B has a denominator which can become zero when both real and imaginary components vanish independently. That is

$$Z'''_B = Z'_B Z''_B/(Z'_B + Z''_B)$$

$$\begin{aligned} Z'_B &= Z'_1 + Z'_2 + Z'_1 Z'_2/Z'_3 \\ &= (R_1 + R_2) + j(R_1 R_2/X_3) \end{aligned}$$

$$\begin{aligned} Z''_B &= Z''_1 + Z''_2 + Z''_1 Z''_2/Z''_3 \\ &= -(X_1 X_2/R_3) - j(X_1 + X_2) \ , \end{aligned}$$

where the real part of Z is R, and the imaginary part is X, in general.

For resonance, the double condition for maximum Z_B is

(I) $\quad \mathrm{Re}\ (Z'_B + Z''_B) = R_1 + R_2 - (X_1 X_2/R_3) = 0$

(II) $\quad \mathrm{Im}\ (Z'_B + Z''_B) = -(X_1 + X_2) + (R_1 R_2/X_3) = 0 \ .$

For the actual double T-network used in the amplifier, the values are $R_1 = 357$ K, $R_2 = 88.7$ K, $R_3 = 73$ K, $C_1 = .005$ μf, $C_2 = .02$ μf, $C_3 = .024$ μf. Either (I) or (II) can be used for determining the resonant frequency under these circumstances, since one condition implies the other if all circuit components are known and compatible. Assuming that $X \to x = 1/\omega_o C$ at resonance, then using the nominal circuit element values,

$$\text{(I)} \quad 1/\omega_o^2 = (R_1 + R_2)\, C_1\, C_2\, R_3 = 3.256 \times 10^{-6} \text{ sec}^2$$

$$\text{(II)} \quad 1/\omega_o^2 = C_1\, C_2\, C_3\, R_1\, R_2/(C_2 + C_1) = 3.050 \times 10^{-6} \text{ sec}^2 .$$

The average of these values gives $f_o = \omega_o/2\pi = 89.6$ Hz, compared with the experimental value of 86.2 Hz. At this frequency, there will also be a theoretical upper limit, A, for the gain.

The general condition for resonance found by eliminating ω_o^2 from (I) and (II) is

$$1/x_3 R_3 = (1/x_1 + 1/x_2)(1/R_1 + 1/R_2) .$$

To simplify computations, introduce the dimensionless parameters, p, q, s, α, which are defined in terms of the impedances at resonance,

$$p = R_1/(R_1 + R_2)$$
$$q = x_1/(x_1 + x_2)$$
$$s = (x_1 + x_2)/(R_1 + R_2)$$
$$\alpha = \omega/\omega_o .$$

Then the values of the circuit components in terms of these parameters are

$$R_1 = p\ R$$

$$R_2 = (1 - p)\ R$$

$$R_3 = \left(\frac{x_1\ x_2}{R_1 + R_2}\right) = q(1 - q)\ s^2\ R$$

$$X_1 = x_1/\alpha = (qs/\alpha)\ R$$

$$X_2 = x_2/\alpha = [(1 - q)s/\alpha]\ R$$

$$X_3 = \left(\frac{R_1\ R_2}{X_1 + X_2}\right) = [p(1 - p)/s\alpha]\ R$$

The Π-network equivalent impedances in terms of these parameters leads to

$$Z'_B = R_1 + R_2 + j\ R_1\ R_2/X_3 = (1 + js\alpha)\ R$$

$$Z''_B = -(X_1\ X_2)/R_3 - j(X_1 + X_2) = -(1/\alpha^2)(1 + js\alpha)\ R$$
$$= -(1/\alpha^2)\ Z'_B$$

$$Z'_A = R_1 - j\ X_3(R_1 + R_2)/R_2 = (p/s\alpha)(s\alpha - j)\ R$$

$$Z''_A = R_3(X_2 + X_1)/X_2 - j\ X_1 = (qs/\alpha)(s\alpha - j)\ R$$
$$= (qs^2/p)\ Z'_A$$

$$Z'_C = R_2 - j\ X_3(R_1 + R_2)/R_1 = [(1 - p)/s\alpha](s\alpha - j)\ R$$

$$Z''_C = -j\ X_2 + R_3(X_1 + X_2)/X_1 = (1 - q)(s/\alpha)(s\alpha - j)\ R$$
$$= \left(\frac{1 - q}{1 - p}\right)\ s^2\ Z'_C$$

Substitution of these values gives the following simplification for the single Π-network equivalent impedances:

$$Z_A''' = [(s\alpha - j)/(\alpha W)]\ R$$

$$Z_B''' = Z_A'''\ [\alpha/(1 - \alpha^2)]\ j\ W = j\ \xi\ W\ Z_A'''$$

$$Z_C''' = (1/s\alpha)\ [(s\alpha - j)]\ B\ R = B\ W\ Z_A'''$$

$$B = s\ [1/(1 - q) + s^2/(1 - p)]^{-1}$$

$$\xi = \alpha/(1 - \alpha^2)$$

$$W = (p + qs^2)/(pqs)$$

$$\alpha = \omega/\omega_o\ .$$

For the second step of formulating a circuit where the Π-network is included with the amplifier, the entire network must be considered. For simplification, however, allow the excitation source and the output system to be totally uncoupled from the tuned amplifier. Figure 13 indicates the relationship between circuit elements and circuit variables. The triple primed quantities on the diagram indicate the equivalent Π-network values for the double T-network. The current through the operational amplifier, which has amplification, A, is

$$I_0 = A\ I_1$$

$$I_0 = I_B + I_C = (V_A - V_C)/Z_B''' - V_C/Z_C'''$$

$$I_1 = I_A - I_B = - V_A/Z_A''' - (V_A - V_C)/Z_B'''\ .$$

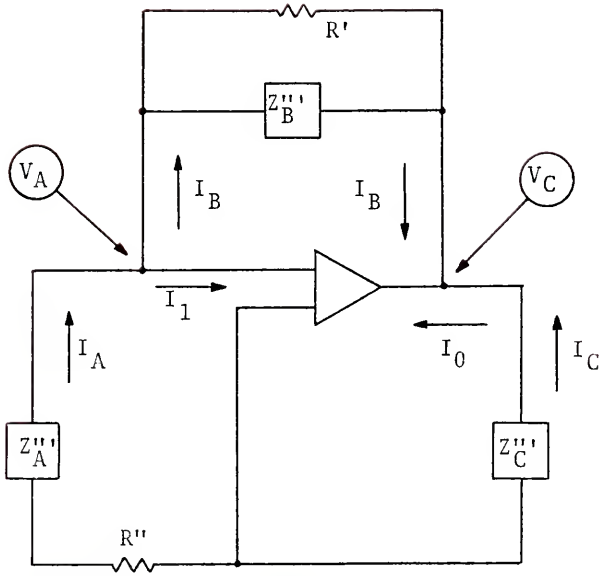

Figure 13. Tuned amplifier circuit model.

Substitution, and collection of terms in V_A and V_C, gives the gain, G, of the system,

$$G = V_C/V_A = A \left(\frac{Z'''_C}{Z'''_A} \right) \cdot \left(\frac{Z'''_B + Z'''_A}{Z'''_B + A\, Z'''_C} \right) .$$

To retain conventional interpretation of a feedback amplifier, introduce an effective amplification, A*, and an effective feedback function, F*,

$$A^* = A\, Z'''_C / Z'''_A$$

$$F^* = Z'''_A / Z'''_B$$

$$G^* = A^*/(1 + A^*F^*) .$$

Then the gain becomes a product of two functions -- effective gain, G*, and a modifier function, (1 + F*) ,

$$G = G^* (1 + F^*) .$$

The insertion of physical resistors at critical locations modifies the gain; for example, in series with Z''''_A or in shunt with Z'''_A , Z'''_B , or Z'''_C . In each case, G* is different. Resistors across Z'''_A or Z'''_B are least influential in the tuned amplifier of U7. However, a resistor of the order of R', $R' = R_1 + R_2$, decreases the gain substantially, and should be modeled into the circuit as a realistic value for the internal resistance of the operational amplifier.

Consider the gain versus frequency characteristic where the resistor R' is included, and let $Z'''_B \rightarrow Z^*'''_B$,

$$Z_B^{*'''} = Z_B''' \; R'/(Z_B''' + R')$$

$$= Z_B' \; Z_B'' \; R'/(Z_B' \; Z_B'' + R' \; Z_B'' + R' \; Z_B') \; .$$

The resonant frequency is shifted with the addition of R', so that new dimensionless parameters are required. Returning to conditions (I) and (II), and requiring that the denominator of $Z_B^{*'''}$ become zero at resonance,

(I') $\quad R' \; [R_1 + R_2 - X_1X_2/R_3] + \beta = 0$

(II') $\quad R' \; [-(X_1 + X_2) + R_1R_2/X_3] + \gamma = 0$

$$\beta = (R_1 + R_2)(-X_1X_2/R_3) + (R_1R_2/X_3)(X_1 + X_2)$$

$$\gamma = -R_1R_2X_1X_2/(X_3R_3) - (X_1 + X_2)(R_1 + R_2)$$

The coefficient of R' represents conditions (I) and (II), whereas β and γ are corrections for shunting Z_B'''. To find the resonant frequency, use X_3 from (II'),

$$X_3 = [R_1R_2/2RR_3]\left(\frac{RR_3 - X_1X_2}{X_1 + X_2}\right) \quad , \quad \text{Case } R' = R_1 + R_2 = R.$$

Substitution of X_3 in (I') gives the relation for the resonant frequency, ω_o,

$$1/\omega_o^4 + \left(R_3^2(C_1 + C_2)^2 - 3 \; R \; C_1C_2R_3/2\right) \; 1/\omega_o^2$$

$$+ C_1^2 \; C_2^2 \; R_3^2 \; R^2/2 = 0 \; .$$

Substituting values for the circuit constants gives

$$1/\omega_o^2 = 3.828 \times 10^{-6} \text{ sec}^2$$

$$f_o = 81.4 \text{ Hertz}$$

The peak of the response is broad, with its center at about 83 Hz when R' = 2 R, experimentally. The corresponding bandwidth is about 20 Hz. These values compare well with f_o = 89.6 Hz calculated for the case of R' = ∞.

The peak gain was lowered from 500 to 270 by the addition of R' = 1 M, which is considered as a justification of the model performance in the vicinity around the tuned frequency. Therefore, in summary, a suitable model for the tuned amplifier U7 consists of a Π-network with Z_A''', $Z_B^{*'''}$, and Z_C''', where $Z_B^{*'''}$ is the effective value of Z_B''' shunted with R' = 1 megohm. A simpler first approximation model would ignore R' (i.e., R' = ∞), but would require the peak response to be reduced by a ratio of $Z_B^{*'''}/Z_B'''$. This simpler model also would indicate correctly an appropriate frequency shift that occurs near maximum gain.

The diminished performance of U7 for varying R'' is very similar to that when R' is varied. This can be shown by taking derivatives of G, letting $\Delta Z_B''' = Z_B^{*'''} - Z_B'''$, and $\Delta Z_A''' = Z_A^{*'''} - Z_A'''$. The result is that R' R'' ∿ constant.

An unusual and unexpected effect in the tuned amplifier performance is a phase shift between input and output which depends on the amplitude of the input signal. The shift was observed for a sinusoidal test signal input, and was approximately linear, 6 degrees over a 10-volt output when the input

was changed over 15 millivolts. For normal d^2 Raman operation, where signal levels of 1 microvolt or less are used, this is an unimportant effect.

Random Noise and Interference

The following list of items have been considered, evaluated or represent modifications leading up to a condition where the Raman lines of carbon tetrachloride are observed with 3 milliwatt laser excitation:

(1) Electrical transients: The insertion of a 1:1 isolation transformer greatly reduces transient interference which comes through the power line into the long time constant stages of the operational amplifiers.

(2) Scan motor switching: Most switches were shunted with a 0.25 μf capacitor. Special low-noise switches instead of conventional wafer switches are suggested, but none were used. Also, judicious relocations of the switches and switched circuits were not attempted.

(3) Intermittent wobble: Some frequency drifting was corrected by changing the natural frequency. Overheating of circuit components was corrected by reducing the modulation power demand. Phase "overcontrol" was corrected by electrically loading the coil with huge capacitors (225 μf). Intermittent mechanical friction between the drive coil and field magnet was corrected by mechanical realignment.

(4) Noise potentiometers: Noise was traced to potentiometer components in the square wave amplifier (U3) and the preamplifier (U5), but the components were not replaced.

(5) Parasitic oscillations: The preamplifier stage required strong negative feedback for the higher frequencies (1 to 10 KHz) -- .01 μf was used for degenerative coupling.

(6) Jitter due to zener diodes: Corrective measures were either to remove them functionally, or to by-pass them with small capacitors.

(7) Operational amplifiers: These units were sometimes unbalanced, or had irregular output in time, or simply "gave up." Four out of eight positions have been replaced with more than four units, although sometimes the units have remained partially effective in operation.

(8) Power supply coupling: Each amplifier or transistor acts as a load to the power supply -- a loading which varies over each cycle. All circuits, particularly the drive circuit with Q4 and Q3, are reduced to a minimum drain required for constant, consistent operation. In this way, variations in the power supply load not only reduce the demand on the power supply regulator so that it works more effectively, but also these variations are less of a disturbance to other circuits located along the line between the load and the regulator. Further isolation from the power supply is provided by RC filters (47 μf x 1 KΩ = 50 ms) at each of the operational amplifier power terminals, including the dc amplifiers in the second detector. Not one unit could be ignored in obtaining

quiet operation. Power supply ripple has been less than 1 millivolt throughout the performance; 1 microvolt sensitivity is required for the Raman signal channel; and ripple following any of the filter units has not been measurable.

Isolation between each stage and the power supply serves as a partial isolation between stages. However, several interstage leads which appeared as printed circuitry on the card were physically removed because they contributed to crosstalk or feedback. An empirical approach to isolation of troublesome circuit elements has reduced the noise level by an order of magnitude.

(9) Feedback: A significant feedback problem exists between the preamplifier and the tuned amplifier due to in-phase feedback between the output and input of the combined two units. If the inverting input of the preamplifier is used for the photomultiplier signal, and a decoupling resistor of 22 K is used between stages, the "noise" is reduced by about an order of magnitude.

Interstage Decoupling

Since the Raman scattering produces small signals, sensitive amplifiers are needed to record them. If an amplifier system contributes too much noise, Raman signals would not be observed. Random noise effects can be integrated out with the use of long time constant circuits over many cycles, but this can only be done when the events are of equal positive

and negative content during the observation time. Interstage coupling can be an effective source of nonrandom noise which cannot be integrated, but since it is identifiable, it can be minimized or eliminated.

For example, consider a 120 Hz ripple in the power supply. If either the wobble frequency, which is derived from the mechanical vibration of the slit, or the 60 Hz power source changes, then a beat frequency is generated. This beat could appear at the chopper, which is located at the juncture of the sync and signal channels, and the second detector would proceed to average out positive and negative rectified portions of the beat frequency wave forms. Since it is not a Raman signal, the beat frequency ideally contributes nothing to the signal channel if all frequencies are constant; but practically, if the input to any stage of the signal channel is not isolated, or balanced with respect to power supply ripple or neutral potential (ground), or both, then the stage accepts the beat signal as a real signal input. The beat frequency therefore appears at the recorder, perhaps as a regular tracing, but generally it is overwhelming to the weak Raman line recording.

Other examples of interstage signal coupling include square wave, fundamental or harmonic frequencies, parasitics, and power line transients. The means of decoupling varied greatly to accommodate the different waveforms. Successful solutions have included negative feedback, resistor damping, isolation, and stabilization (thermal and frequency).

CHAPTER IV

RESULTS AND DISCUSSION

The circuitry and instrumentation described in Chapters I and II allow for the detection of a Raman spectrum of carbon tetrachloride, as shown in Figure 14. This is a poor Raman spectrum, but it permits evaluation of the d^2 method. Generally speaking, the Raman lines for carbon tetrachloride are strong lines, appearing with wavenumbers of 217 (70), 313 (80), 459 (100), 760 (20) and 791 (20) cm^{-1}, the parenthetic numbers indicating relative intensity at 4358 Å excitation [18]. These Raman lines correspond to Stokes lines at 6416, 6456, 6517, 6648 and 6661 Å using helium-neon laser excitation. Figure 14 is very similar to that obtained by Darling and Williams, who used much stronger excitation, and obtained corresponding Stokes lines of 4932, 4956, 4992, 5068 and 5076 Å with argon laser excitation. For reference and identification, a characteristic d^2 profile of a highly attenuated primary 6328 Å line is shown in Figure 15.

Figure 14 shows a series of reasonably sharp features which are spectral lines, or specifically their d^2 equivalent. The largest features are marked A to K with wavelengths as shown in Table I. The position of the Stokes lines of carbon tetrachloride is also shown, and designated a to k. They

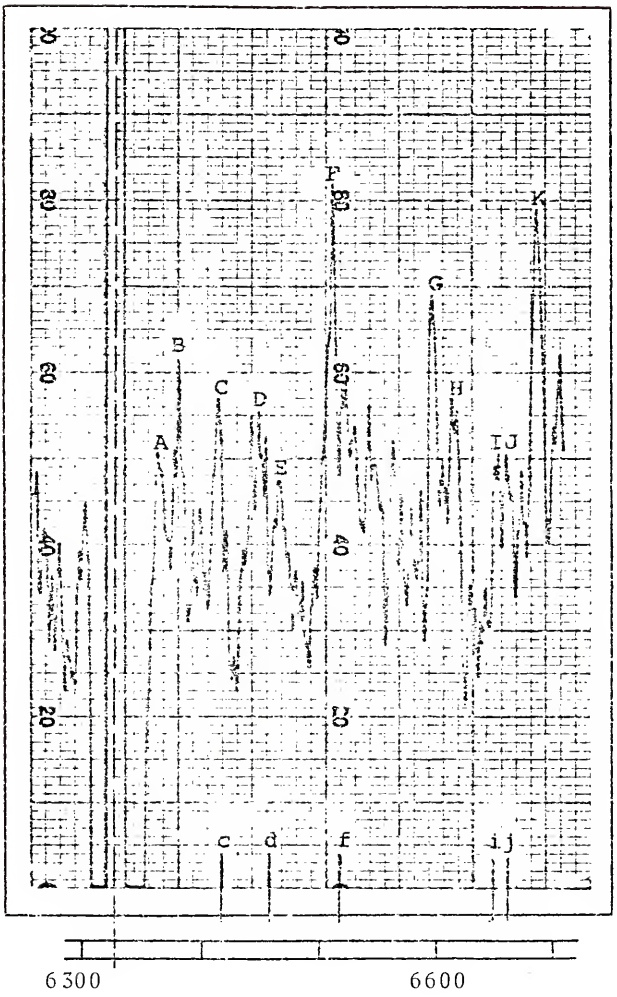

Figure 14. Initial d^2 Raman spectrum of carbon tetrachloride, 3 mw 6328 Å.

Table I

Features Appearing in Figure 14

	Observed Wavelength	Δλ		Calculated Stokes Wavelengths	Δλ
A	6358 (11)	30	a	--	--
B	6380 (15)	52	b	--	--
C	6414 (25)	86	c	6416 (70)	88
D	6448 (14)	120	d	6456 (80)	128
E	6467 (12)	139	e	--	--
F	6512 (37)	184	f	6517 (100)	189
G	6597 (30)	269	g	--	--
H	6616 (20)	288	h	--	--
I	6650 (13)	323	i	6648 (20)	320
J	6660 (11)	332	j	6661 (20)	333
K	6686 (38)	358	k	--	--

Notes: (1) The amplitudes of the observed lines as they appear in Figure 14 are shown in parentheses. The scale is chart units.

(2) Δλ is the difference between excitation wavelength and observed wavelength in Å.

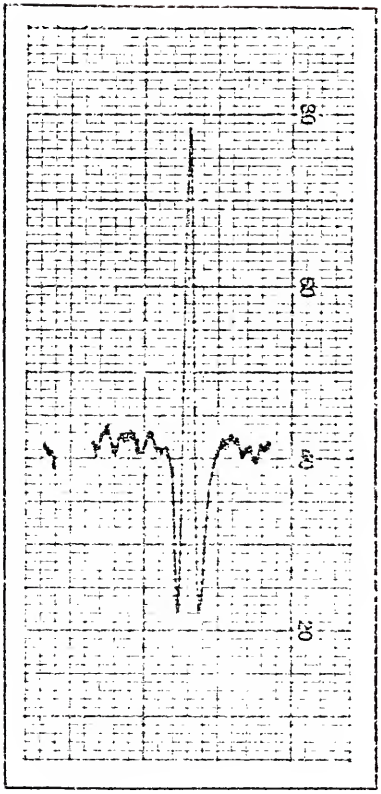

Figure 15. Typical d^2 line response.

also appear in the table. It is evident that the calculated Stokes lines c, d and f fall near large features of the spectrum, namely the features C, D and F, respectively. On the other hand, the features A, B, E, G, H and K which are observed are not predicted as Raman derived lines of carbon tetrachloride. Stokes lines i and j, which in fact may be concluded to appear in the spectrum, are of low intensity as predicted from the literature.

Wavelengths of lines can be determined directly from the recorded data of Figure 14 by establishing a scale in units of chart divisions. Eight chart divisions cover precisely 100 Å, so that the wavelength of an arbitrary line is determined by adding or subtracting from 6328 Å, the laser excitation indicated by the broken line. Wavelength scales indicated on the figures are, therefore, only approximate.

Within some error limits, the large number of features that appear in Figure 14 could perhaps match peaks of any known spectrum, although there is apparently excellent agreement in wavelength and intensity with predicted values for some specific peaks. For this reason, it would be desirable to seek confirming data that C, D and F of Figure 14 are in fact Raman lines in the carbon tetrachloride or sample spectrum. Consider the following arguments:

a) Apparent Raman spectra may occur because of other scatterers, where any feature that appears in the data could be properly ascribed to the illumination source or to the instrumentation. For example, helium and neon spectral lines

may be elastically scattered; such scattering would produce Rayleigh lines of the laser gas with an intensity that could be high enough to produce features as large as those of Figure 14.

b) Corresponding to each Stokes line of any Raman spectrum, on the long wavelength side of the laser line, an anti-Stokes line should also appear on the short wavelength side, with a difference in wavelength from the laser light which departs in a predictable manner from the difference observed for the Stokes line. Features failing to show this difference in separation from the laser light might be expected to originate from imperfections of the grating. Such features, commonly referred to as "ghosts," are well known to be characteristic of ruled gratings, and presumably also of replica gratings from the ruled gratings. Their intensity is normally negligible, but might be sufficient to show up here.

Both of the possibilities were investigated as described below. With reference to the anti-Stokes lines, it is important to note that the Stokes and anti-Stokes lines are different in amplitude as well as wavelength. For example, apparently the origin of the Raman spectrum is a nonlinearity of the molecular polarization, p, with applied electric field, E. Bulk polarization per unit volume, P, is an observable, the average of all molecular polarization, $P = \langle np \rangle$, and can be defined as the difference between electric displacement, D, and the applied electric field,

$$P = (D - \varepsilon_o E)/4\pi$$

$$p = E\,[\varepsilon_o(k - 1)/4\pi n]\,, \qquad \varepsilon/\varepsilon_o = k$$

$$= \langle\alpha\rangle E\,.$$

$\langle\alpha\rangle$ is then an average molecular polarizability, where k is the dielectric constant of a bulk of the material. For a point charge model of a molecule, the dipole formed by charges +q and -q at a separation distance d gives an electric field at large r,

$$E_r \cong 2\,q\,\Delta r/r^3 = 2\,q\,p\,\cos\,\theta/r^3$$

$$= 2\,p/r^3$$

$$p = |q|\,d$$

$$\theta = 0, \text{ for all binary encounters.}$$

For such an approximation, the molecular polarizability is

$$\alpha \cong p/E_r = r^3/2\,.$$

For a general case where the charge is distributed in space, however, assume that $\alpha = \alpha(r)$, and that a Taylor expansion is possible around the equilibrium position, r_o,

$$\alpha(r) = \alpha_o + (\partial\alpha/\partial r)_o\,r + \ldots .$$

Classical electromagnetic theory gives the radiated energy, I, as

$$I = 2[d^2\,P/d\,t^2]/3\,c^2\,.$$

To formulate the time dependence of the polarization on time-varying fields, the excitation is $E = E_o \cos \nu t$. The dipole oscillates with a frequency ν' about r_o, and $r = r_o \cos \nu' t$. Then

$$P = \left(E_o \cos \nu t\right) \left(\alpha_o + (\partial\alpha/\partial r)_o \, r_o \cos \nu' t + \ldots\right)$$

$$= \left(E_o \, \alpha_o \cos \nu t\right) + E_o r_o/2 \left((\partial\alpha/\partial r)_o [\cos(\nu - \nu')t + \cos(\nu + \nu')t] + \ldots\right) .$$

The first term accounts for the Rayleigh scattering, the second for Stokes and the third for anti-Stokes scattering of the incident radiation. Higher order terms exist, but each order with less amplitude.

The anti-Stokes components represent higher energy photons than the exciting photons. This is because the molecule originally is in an excited state and drops to a ground level after the photon collision. The classical radiation depends on the fourth power of the frequency, so that the ratio of the intensity of the Stokes line is

$$\frac{\text{anti-Stokes}}{\text{Stokes}} = \left(\frac{\nu + \nu'}{\nu - \nu'}\right)^4 e^{-h\nu'/kT} .$$

The Stokes bands (lower frequency) are always the stronger. For carbon tetrachloride, for example, the use of the Stokes bands at room temperature should give increased intensity by factors of 1.11, 1.17 and 1.26 for the Raman lines 217, 313 and 458 cm^{-1}.

Carbon Tetrachloride versus Toluene

After obtaining the Raman spectra data of Figure 14, the system was changed -- optimized to make a comparison between carbon tetrachloride and toluene Raman spectra. Figures 16, 17, 18 and 19 show the results of runs which cover the Stokes and anti-Stokes ranges of each material. Except for changing the material in the scattering cell, all instrumentation conditions remained identically the same for both runs, but different from Figure 14.

Five toluene lines in the anti-Stokes spectrum were identified and marked A, B, C, D and E in Figures 16 and 17 -- 6134, 6037, 5958, 5490 and 5888 Å. According to the literature [24], the dominant lines in the region should be 6126, 6028, 5949, 5941 and 5879 Å, which correspond to wavenumbers 521 (15), 786 (43), 1004 (91), 1030 (26) and 1208 (26) cm^{-1}. The lines were identified by using data from both Stokes and anti-Stokes sidebands, and exploiting an asymmetry in wavelength difference between observed wavelength and excitation wavelength. Equal displacements for the Raman Stokes and Raman anti-Stokes lines cannot occur because frequencies are additive, not wavelengths. Other observed "lines" are remarkable in that they are displaced the same amount above and below the excitation wavelength of 6328 Å. Furthermore, it is also remarkable that the equally displaced lines have similar amplitudes on both sides of 6328 Å where the photomultiplier characteristic is known to vary rapidly -- 3% quantum

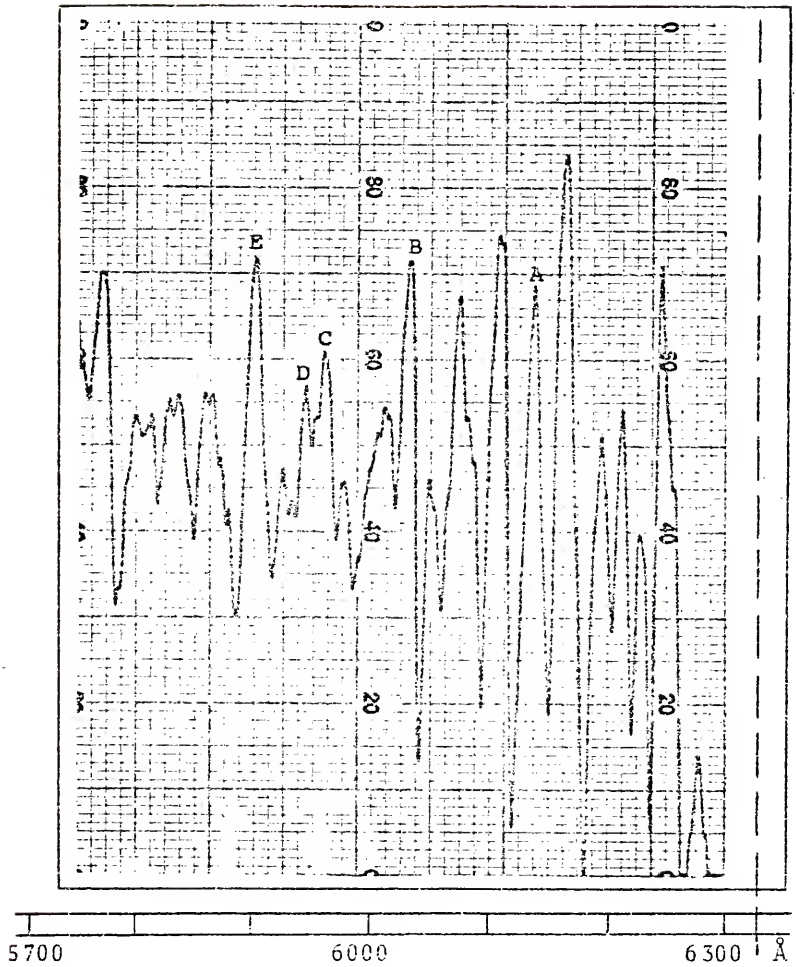

Figure 16. Toluene, Raman anti-Stokes spectrum, 3 mw helium-neon laser 6328 Å.

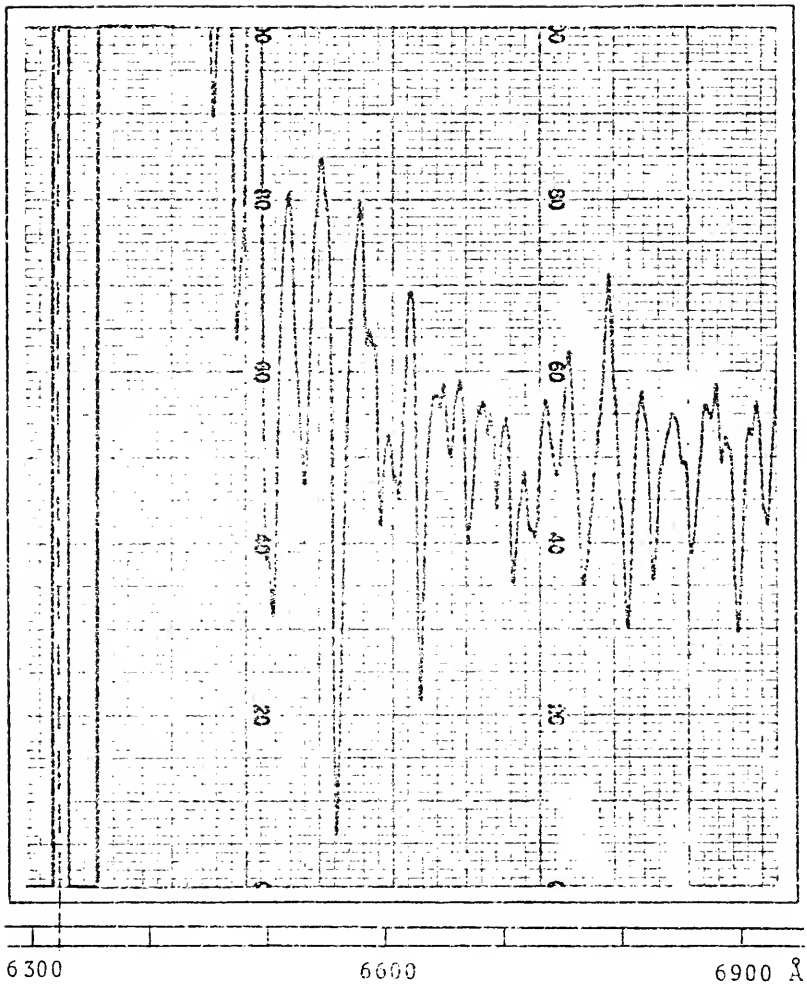

Figure 17. Toluene, Raman Stokes spectrum, 3 mw helium-neon laser 6328 Å.

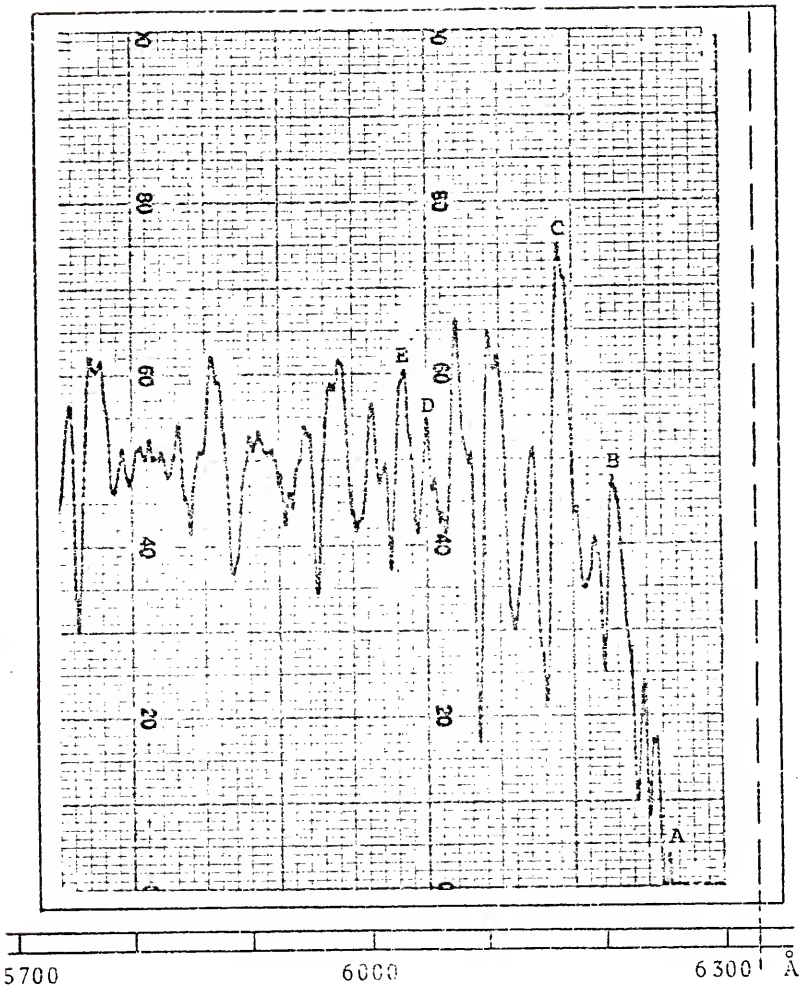

Figure 18. Carbon tetrachloride, Raman anti-Stokes spectrum, 3 mw helium-neon laser 6328 Å.

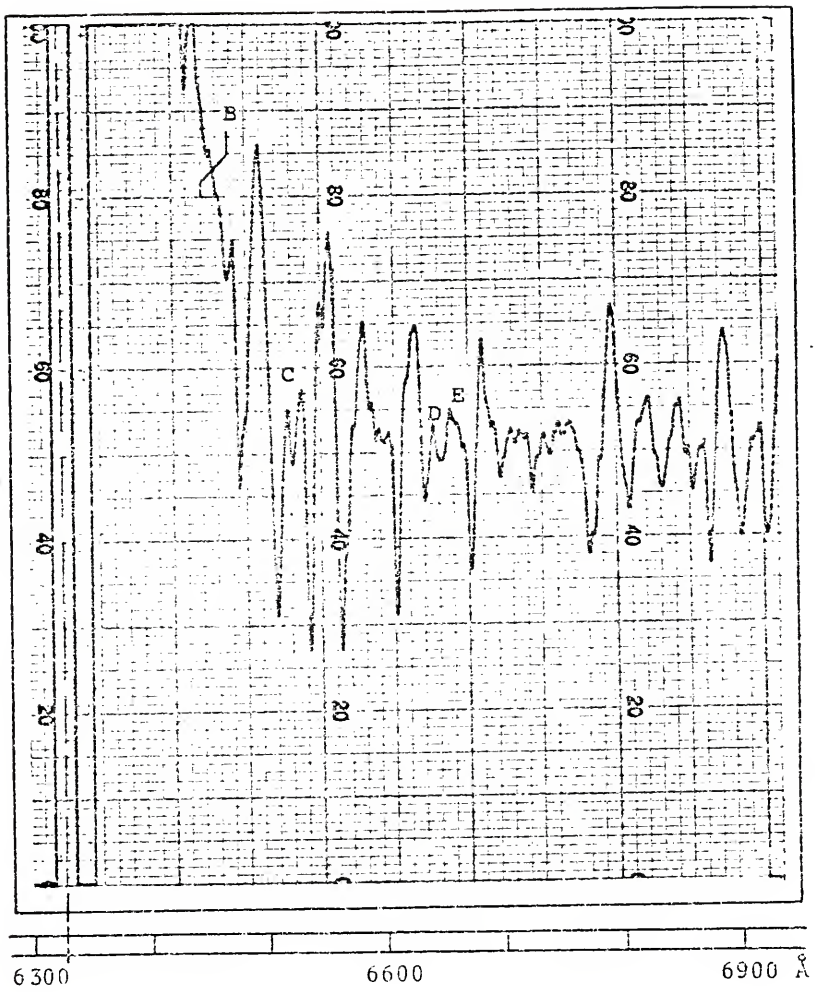

Figure 19. Carbon tetrachloride, Raman Stokes spectrum, 3 mw helium-neon laser 6328 Å.

efficiency at 5828 Å (500 Å below) to <0.1% at 6828 Å (500 Å above the excitation).

Reduction and interpretation of the data are, therefore, difficult because of the interfering "lines" which are interspersed with the Raman spectrum. If Figure 16 (anti-Stokes) and Figure 17 (Stokes) could be superimposed with the aid of a fictitious mirror with properties which (a) folded the two figures so that the 6328 line, λ_o, became the origin for the differential Stokes wavelengths, $(\lambda_s - \lambda_o)$, and differential anti-Stokes wavelength, $(\lambda_o - \lambda_a)$, displacements, and (b) flipped the folds over to match the curved base line of the d^2 recorded pattern, then each of the d^2 spectrum lines would still remain unmatched. This is because the top of a line has "one peak," and the bottom of the line has "two peaks" as shown in Figure 15 -- i.e., an overlay would also be difficult to interpret.

However, an equivalent superposition can be carried out using the tables constructed below, which reduces the data of Figures 16 through 18. Estimates of peak amplitudes are based on a mean measure from the top of a d^2 line (maximum position) to the bottom of a d^2 line (mean minimum of two positions). This is not a very satisfactory amplitude determination for a complicated spectrum, but at least it keeps track of large and small features.

A display of the toluene data in Table II appears in Figure 20; similarly, carbon tetrachloride data of Table III appear in Figure 21. There are lines within each set of

Table II

Light Intensity in the Stokes and Anti-Stokes Regions of Figures 16 and 17 for Toluene

Anti-Stokes		Stokes	
(λ_a)	$(\lambda_o - \lambda_a)$	(λ_s)	$(\lambda_s - \lambda_o)$
5768 (25)	560	6466 (>10)	138
5798 (15)	530	6492 (>36)	164
5831 (12)	497	6520 (40)	192
5865 (20)	463	6547 (57)	219
5888 (38)	E 440	6581 (≈28)	253
5923 (08)	405	6607 (08)	279
5940 (10)	D 388	6612 (28)	284
5958 (15)	C 370	6646 (13)	318
5966 (08)	362	6668 (18)	340
6007 (15)	321	6685 (13)	357
6037 (42)	B 291	6704 (13)	376
6049 (22)	279	6722 (09)	394
6071 (41)	257	6740 (11)	412
6104 (61)	224	6759 (20)	431
6134 (57)	A 194	6793 (38)	465
6160 (74)	168	6820 (27)	492
6192 (28)	136	6848 (16)	520
6207 (29)	121	6883 (22)	555
6246 (>70)	82	6917 (19)	589
6276 (>14)	52		

Notes: (1) Letter designation corresponds with letters on the figures.

(2) Designated lines are the closest match in amplitude and frequency to Stokes sidebands for published Raman modulation frequencies.

(3) Stokes lines are weaker than the anti-Stokes lines due to the photodetector sensitivity in this range. They are too small to be identified.

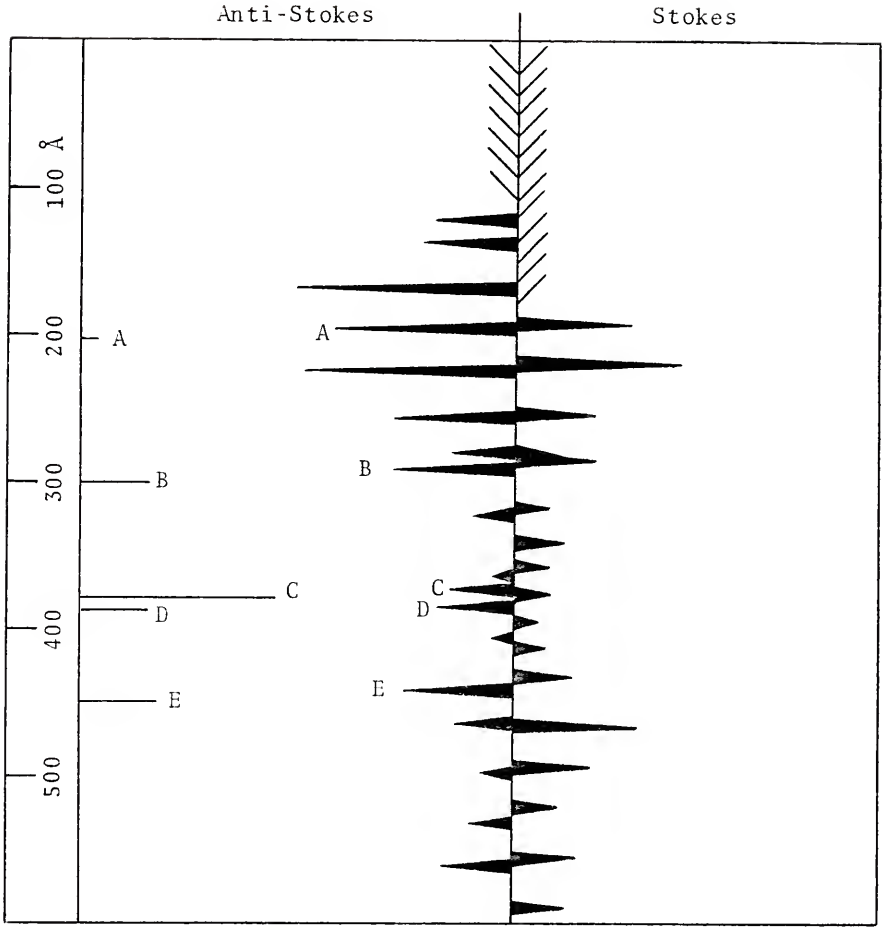

Figure 20. Amplitude of apparent lines on the Stokes and anti-Stokes sides of 6328 Å excitation for toluene (Ref. Figures 16 and 17, and Tables II and IV).

Table III

Light Intensity in the Stokes and Anti-Stokes Regions of Figures 18 and 19 for Carbon Tetrachloride

Anti-Stokes		Stokes	
(λ_a)	$(\lambda_o - \lambda_a)$	(λ_s)	$(\lambda_s - \lambda_o)$
5694 (19)	571	6441 (>08)	113
5704 (22)	549	6460 (>06)	B 132
5790 (04)	538	6472 (05)	144
5838 (09)	490	6496 (48)	168
5868 (22)	460	6517 (10)	C 189
5944 (15)	384	6531 (14)	203
5968 (24)	360	6536 (03)	208
6001 (11)	327	6556 (59)	228
6013 (05)	315	6584 (17)	256
6029 (20)	E 299	6624 (26)	296
6048 (13)	D 280	6642 (04)	D 314
6074 (37)	254	6660 (05)	E 332
6106 (37)	222	6686 (21)	358
6142 (24)	186	6694 (06)	386
6162 (47)	C 166	6792 (26)	464
6191 (11)	137	6822 (12)	494
6209 (29)	B 119	6849 (10)	521
6229 (14)	99	6870 (09)	542
6244 (18)	A 84	6891 (25)	563
6252 (>04)	76	6916 (11)	588

Notes: (1) Letter designation corresponds with letters on the figures.

(2) Unlike the toluene data, these carbon tetrachloride data lines can be seen in the Stokes region because they are nearer to the excitation frequency where the photodetector sensitivity is greater. The amplitudes, nevertheless, are small.

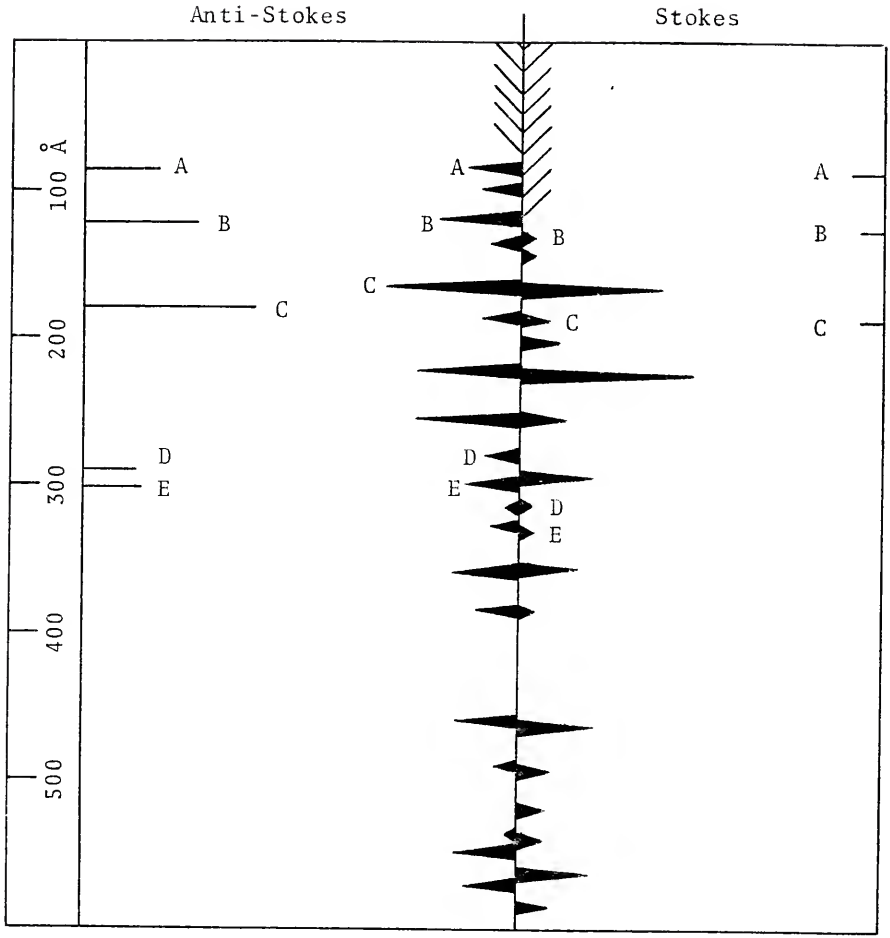

Figure 21. Amplitude of apparent lines on the Stokes and anti-Stokes sides of 6328 Å excitation for carbon tetrachloride (Ref. Figures 18 and 19, and Tables III and IV).

data which have the same frequency difference around the laser center frequency, as well as unmatched lines which are Raman derived. On these figures, Stokes lines appear to be "shifted" from the anti-Stokes lines, but fit expected patterns for Raman spectra, while the interference patterns do not.

Apparently the origin of the interfering lines, therefore, is not Raman scattering, nor Rayleigh scattering of the neon laser line background. The most plausible assumption is that the particular grating has a type of "ghost" which results from a periodic error in the otherwise regular spacing between the ruled lines. This effect is generally small, and is not objectionable. It has an apparent amplitude here of about $1:10^3$ to allow for the Rayleigh line to be the size of the Raman line. This type of "ghost" and others have been long known [25,26].

The grating "ghost effect" should vary with the particular grating in use, but any effect should be reduced substantially if an optical blocking filter for 6328 Å, or the excitation frequency, were inserted between the exit slit and the photomultiplier. Choice of bandwidth for the blocking filter would be governed by the proximity of the Raman line to the laser line, and choice of attenuation would be governed by the "mortal size of the ghost." No filters were available to reduce this interference here at the time of this measurement.

Table IV

Calculated Wavelengths Using Published Frequencies

Wavenumber (cm^{-1})	Anti-Stokes (λ_a)	($\lambda_o - \lambda_a$)	Stokes (λ_s)	($\lambda_s - \lambda_o$)
		Carbon Tetrachloride		
217 (70)	6242 (80)	086	6416 (46)	088
313 (80)	6206 (77)	122	6456 (37)	128
459 (100)	6148 (235)	179	6517 (35)	189
760 (20)	6038 (155)	290	6648 (03)	320
791 (20)	6026 (103)	302	6661 (03)	333
		Toluene		
521 (15)	6126 (22)	202	6544 (03)	216
786 (43)	6028 (95)	300	6660 (03)	332
1004 (91)	5949 (279)	379	6758 (03)	430
1030 (26)	5941 (78)	387	6770 (01)	442
1208 (26)	5879 (106)	449	6851 (01)	523

Notes: (1) The amplitudes have been corrected for frequency (reported excitation was 4358 Å), and also corrected for the photomultiplier response for each frequency.

(2) The photomultiplier correction indicates that the anti-Stokes side is the more intense for 6328 Å excitation.

Slit Modulation and Stability

Both the amplitude and the phase change during operation of the modulator, and this action contributes to a recorder response, although in different ways. A frequency stability of one part in 2.7×10^4 cycles has been attained with the present mechanical system. This is good, but not especially satisfactory because a line scan takes a relatively long time of 0.5 minutes (1350 cycles). Such a variation represents an uncertainty of 5% in Raman line amplitude due to a so-called "stable frequency." Similar change occurs in the noise level (i.e., where no Raman signals are present), so that the recorder can experience amplitude excursions which depend on frequency change as well as crosstalk.

In the present device, modulation amplitude is controlled by a feedback system, where (a) the damping time is uncontrolled, and (b) crosstalk from the master oscillator feedback signal enters both the sync channel and the signal channel. Since the feedback is necessarily of different phase from the sensor, and since the feedback phase varies according to modulator needs, crosstalk effectively produces noise. The modulator circuit is basically stable, but improvement is possible, desirable, and would directly influence the d^2 Raman Spectrometer sensitivity.

To avoid the mechanical modulator problems, it may be possible to consider the use of an all-electric one. Such a device does not exist at present, but could be developed.

For example, immediately after the second spectrometer slit place a light amplifier element consisting of a photosensitive surface which emits electrons. These electrons would pass through an electric or magnetic field which is energized at the wobble frequency. If the electron trajectories were displaced in such a way as to scan a sensitive surface (e.g., a channeltron or electron multiplier), the electron beam wobble would then replace the light beam wobble.

The important point to remember is that an effective scan over the line profile is required, and not just an on-off switch for the detector. In fact, it may be possible to use a conventional photomultiplier if it can be modulated by an external magnetic field up to a critical point where the detector output remains independent of the position of a light spot over its sensitive surface.

If an all-electric modulator were available, the limitation imposed by the inertia or material coefficients of the mechanical modulator would be removed. Frequency changing, including electrical synchronous operations, are readily available by state-of-the-art means. There is also the possibility of extending control with this method into the pulse counting regime for high intensity signals by control of the light amplifier sensitivity. Apparently pulse counting techniques at high signal intensities are desirable for computer purposes, but are very difficult to handle because too many pulses jam the counters [8].

Modified Sync Channel and Second Detector

Development of this d^2 Raman Spectrometer has been hampered by crosstalk from the square wave amplifier output, and in fact the square wave may not be essential to the d^2 Raman operation. The purpose has been to supply a precisely gated "chopper" signal to select out from the tuned amplifier the cosine component which eventually appears at the second detector (recorder). Consider an optional method which uses cosine waveforms throughout as sketched in Figure 22.

For example, it is possible to use a second analog device such as the AD/426 already mentioned, as a substitute for the doubler function. The cosine waveform from the sensor would be used as an input, and the same waveform as a second input, so that multiplication of the input from both sources would be the equivalent of a mathematical "squaring" operation. The output contains an ac term of double frequency, and a dc term which is blocked by a capacitor. Proper phase control of the squarer output means that, at the electron multiplier (or photodetector), only cosine terms are eventually selected.

A third AD/426 device, or its equivalent, could also be substituted for the "chopper" function proper. If the $\cos(2\omega t)$ output from the squarer were one of the inputs, and the other input came from the tuned amplifier, then an analog multiplication operation would result in the product of the cosine component of the photodetector and the reference $\cos(2\omega t)$ function.

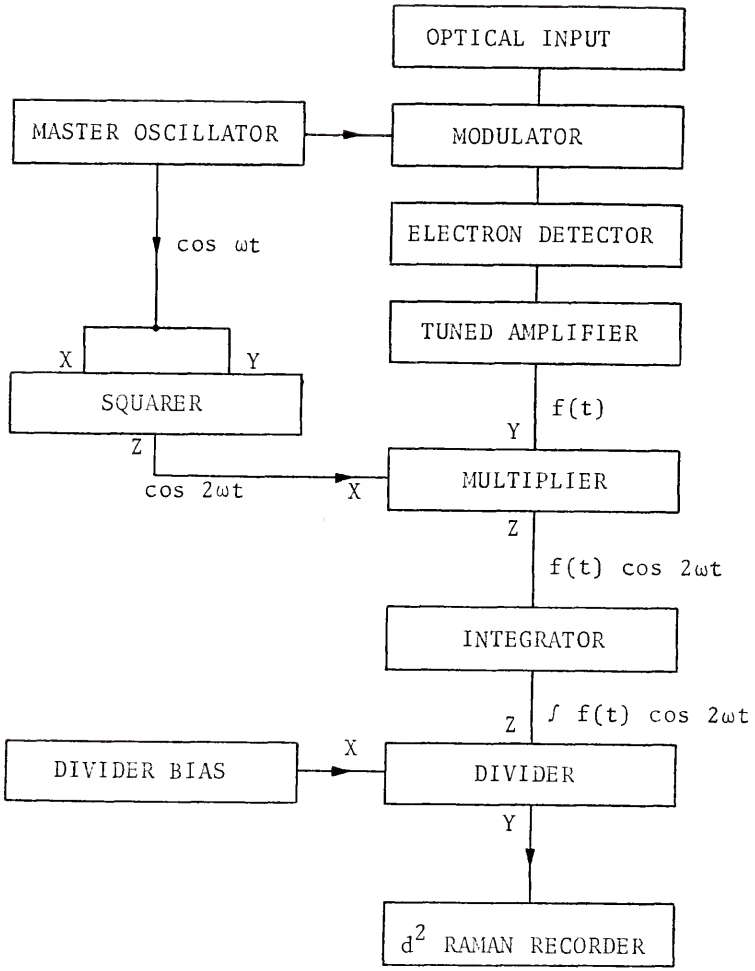

NOTE: (X)(Y) = (Z)

Figure 22. Raman Spectrometer, proposed option.

Furthermore, if the output from the multiplier is integrated, by the use of long time-constant components, the mathematical result would be proportional to the amplitude of the second harmonic cosine terms -- i.e., a second Fourier coefficient of the line profile which appears at the output of the photodetector.

The amplitude of the signal which appears at the photodetector is proportional to $I(x)$, $x = x(t)$ as discussed in Chapter I. Development of $I(x)$ into component terms allows the identification of second harmonic cosine terms, where the Fourier coefficient contains the derivative contributions, d^2, d^4, d^6, etc. In this optional "Fourier" method with AD/426 analog devices, the mathematics is exactly equivalent to the d^2 square wave "chopper" method. Only the electronic technique is different, potentially capable of producing much quieter operating instrumentation with less noise background.

CHAPTER V

SUMMARY AND CONCLUSIONS

Conclusions for this experimental study of d^2 Raman Spectroscopy fall into essentially two categories, one which records the state of d^2 development at the time that the Raman spectra were observed, and another which puts forth an estimate for improved instrumentation based on results from the study.

Raman spectra observed before and after the investigation show that a reduction in background noise can be accomplished by changes in the electronic circuitry. An improvement of about four orders of magnitude in the background level has permitted at least three carbon tetrachloride and three toluene Raman lines to be observed with a weak helium-neon laser of 3 milliwatts. Apparently moderate background levels still exist, and are attributable to circuitry, but it is more fruitful now to redesign the entire system where location of parts, couplings and components are made according to improvements based on present performance.

In general, the photomultiplier has not been a major source of noise, but has limited the Raman signal response. The present unit has a quantum efficiency of 0.8% at 6328 Å, which could be changed to one with about 15% efficiency.

Electronic coupling between amplifier stages has presented a major difficulty because levels of less than 1 microvolt interference are required. Operational amplifiers and transistor circuits have been altered to offer minimum loading to the power supply, thus reducing inductive coupling in closed loop circuits, and capacitive coupling in open circuits. In addition to the interstage coupling, an associated coupling has been found between operational amplifiers and the power supply. This coupling has served both to introduce power supply ripple into the signal channels, and to allow variations in one stage to be conducted through the hard wiring as an interference signal to another stage. A successful buffer scheme has been devised which uses a series resistor with capacitors across the amplifier power leads at each individual amplifier. The time constant is as large as possible, 47 ms (47 μf x 1 K), twice the wobble period. Buffering of all the amplifiers was needed, and succeeded so that contributions from the power supply ripple of 1 millivolt in 15 volts became relatively ineffectual.

Electrical noise sources have been traced variously to multiple ground loops, switches, potentiometers and thermal excursions. Insofar as possible, contributions from the noise sources have been minimized by physical isolation or replacement of components.

Modulator interference has been difficult to isolate from the amplifier stages. The modulator feedback loop includes a powerful transistor driver which is energized at

a phase that depends on an error signal for synchronism. The error depends on wobble amplitude and frequency, which in turn depend on the wobbler material coefficients. The entire modulator then becomes responsive to ambient air currents, temperature, power supply coupling and circuit feedback. Nevertheless, the frequency has been stabilized to one part in 2.7×10^4. Decoupling and reduction of the modulator power have made a major reduction in the background noise.

A tuned amplifier is essential to the present system. The particular type of tuned amplifier circuit is a double T-network which is basically an active filter circuit. Performance and analysis indicate that the feedback, input and output circuits are unnecessarily dependent, and could be improved if at least the feedback circuit included a buffer for decoupling.

The Raman spectra have been influenced by optical component performance -- "ghosts" due to grating imperfection (periodic ruling line variation effect), and contributions from the neon background of the helium-neon laser. Both of these optical difficulties apparently can be remedied with filters; line transmission filter at the entrance slit, and line blocking at the exit slit.

The present system would probably give excellent Raman spectra if a 50 mw argon laser were used, and if a blocking filter for 4880 Å were inserted between the exit slit and the photomultiplier. Assuming that the electronic noise background remains constant, the change to 4880 Å improves the

photomultiplier efficiency 10/0.8 = 12.5 X, radiation efficiency $(6328/4880)^4$ = 2.83 X, power input 50/3 = 16.7 X, giving an overall improvement of 592 X. The noise level therefore would be approximately 1.6% of the Raman line 459 cm^{-1} of carbon tetrachloride. Without the blocking filter, however, the grating imperfections would contribute interference lines as large as the Raman lines.

An optional design for a d^2 Raman Spectrometer is proposed which uses analog electronic devices to "square," "multiply," and integrate the output from a photodetector. The method uses quiet low level sinusoidal signals, and the mathematical orthogonal property of a Fourier integral to select out the second harmonic coefficient, which in turn approximates the d^2 profile of the Raman line. The method does not require a tuned amplifier, although its use could help noise rejection. The method is also compatible with a proposed all-electric wobbler sampling technique.

APPENDIX A

WAVEFORMS OF SELECT POSITIONS IN ELECTRONIC CIRCUITS OF d^2 RAMAN SPECTROMETER

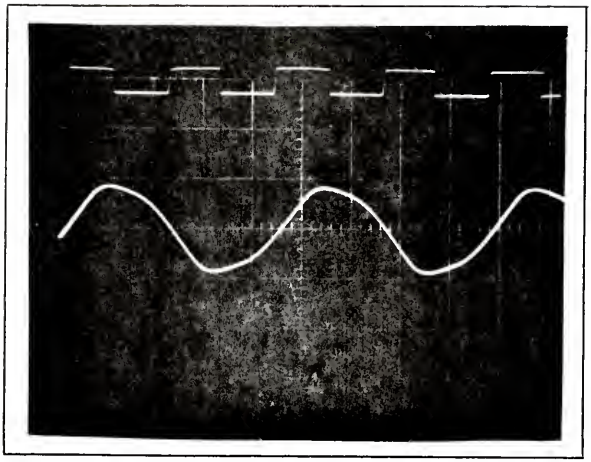

Figure 23. Modulator, sensor amplifier output, U2 (10 volt/cm x 5 ms/cm).

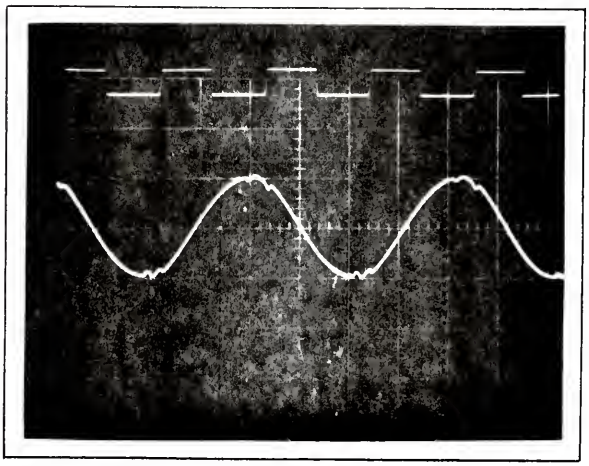

Figure 24. Master oscillator output, U1 (1 volt/cm x 5 ms/cm).

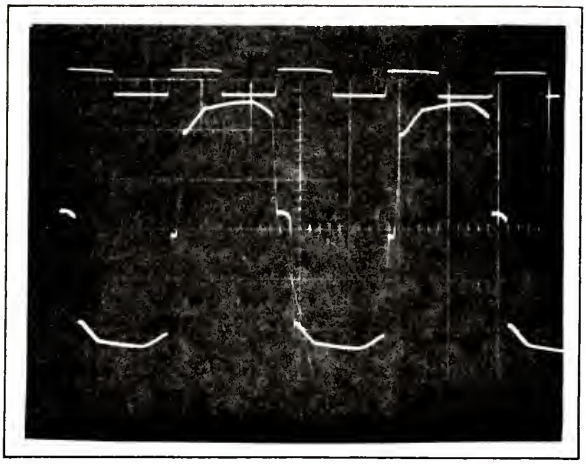

Figure 25. Modulator, driver output to coil, Q4 (0.2 volt/cm x 5 ms/cm).

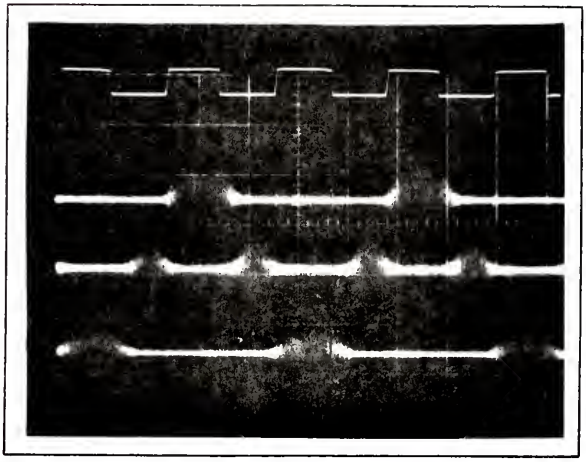

Figure 26. Signal channel, preamplifier output, U5 (0.2 volt/cm x 5 ms/cm). A - right wing of optical line, B - optical line center, C - left wing of optical line.

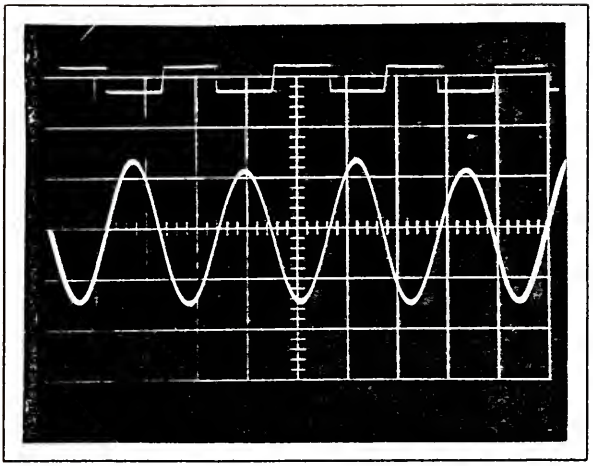

(a) Optical line center

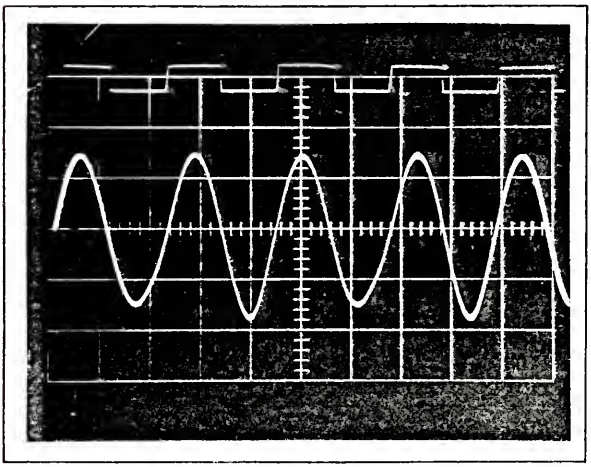

(b) Optical line wing

Figure 27. Signal channel, tuned amplifier output, U7 (5 volt/cm x 5 ms/cm).

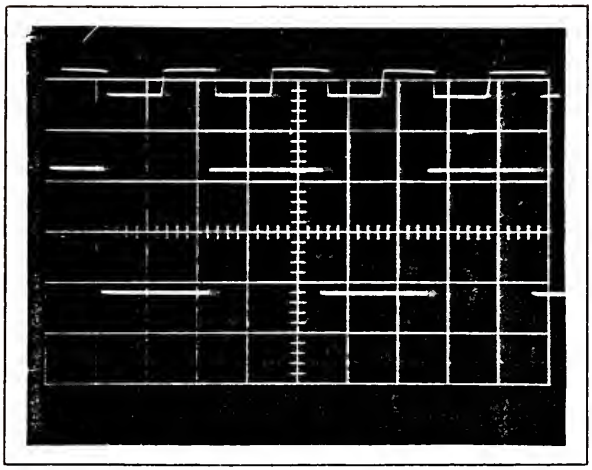

Figure 28. Sync channel, square wave amplifier output, U3 (10 volt/cm x 5 ms/cm).

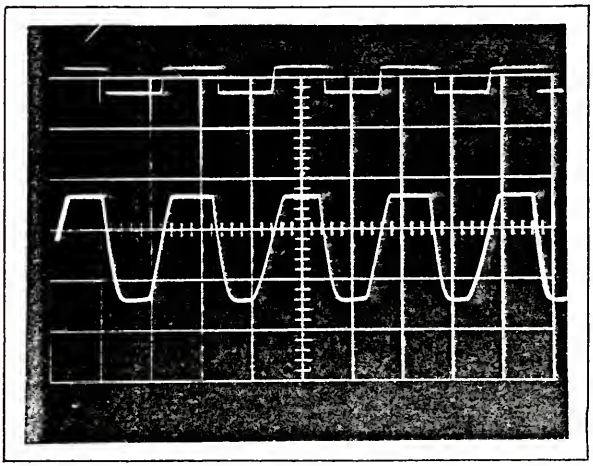

Figure 29. Sync channel, doubler output, U4 (0.5 volt/cm x 5 ms/cm). Unequal rise and fall times are due to different RC time constants in the wave shape generation.

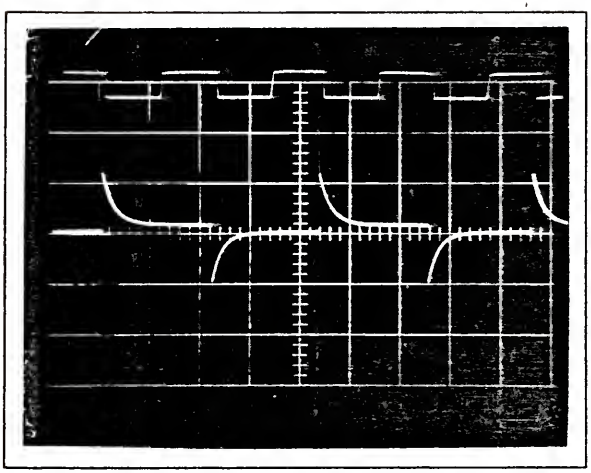

(a) Total input

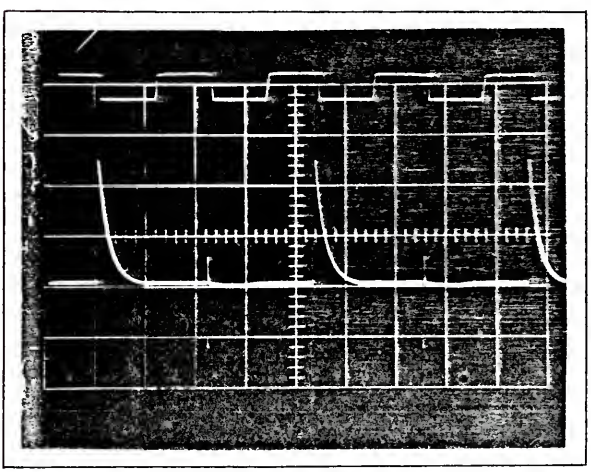

(b) Inverting input only

Figure 30. Sync channel, doubler amplifier input, U4 (10 volt/cm x 5 ms/cm, total input; 5 volt/cm x 5 ms/cm, inverting input).

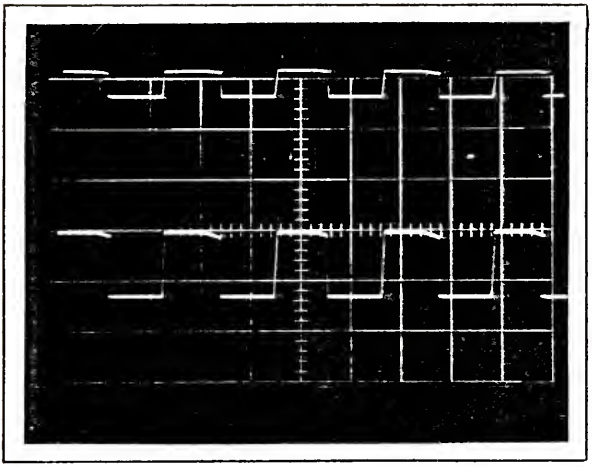

Figure 31. Sync channel, doubler amplifier output, U6 (10 volt/cm x 5 ms/cm).

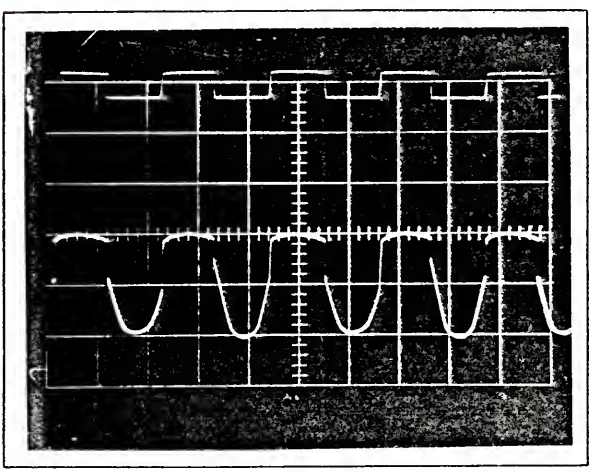

Figure 32. Second detector, rectified tuned amplifier output, U8 input (5 volt/cm x 5 ms/cm).

BIBLIOGRAPHY

1. Williams, D.T., "Spectrometer System," U.S. Patent 232,053, March 6, 1972.

2. Hager, R.N., Jr., The Theory, Design and Application of a Second Derivative Spectrometer, Ph.D. dissertation, University of Florida, 1970.

3. Spectrometrics of Florida, Inc. (subsidiary of ABA Industries, Inc.), P.O. Box 517, Pinellas Park, Florida 33565.

4. Lear Siegler, Inc., 1 Inverness Drive East, Englewood, Colorado 80110.

5. Darling, J.W. II, "The Application of a d^2 Spectrometer for the Detection of Raman Spectra," paper presented at the Southeastern Regional Student Conference, Atlanta, Georgia, April 18-19, 1974.

6. Freeman, S.K., Applications of Laser Raman Spectroscopy, John Wiley and Sons, 1974.

7. Panofsky, W.K.H. and Phillips, M., Classical Electricity and Magnetism, Addison-Wesley, 1962.

8. Anderson, A., The Raman Effect, Volume 1: Principles, Marcel Dekker, Inc., 1971.

9. Sushchinskii, M.N., Raman Spectra of Molecules and Crystals, Israel Program for Scientific Translations, 1972.

10. Tobin, M.C., Laser Raman Spectroscopy, Wiley Interscience, 1971.

11. Spectra Physics, 1250 W. Middlefield Road, Mountain View, California 94040.

12. Jarrel-Ash, 590 Lincoln Street, Waltham, Massachusetts 02154.

13. EMI Electronics Ltd. (Distributors Whittaker Corp., Gencom Division, 80 Express Street, Plain View, Long Island, New York).

14. Linear Integrated Circuits and MOS Devices, RCA Solid State Series, 1972.

15. Analog Devices, Route #1, Industrial Park, P.O. Box 280, Norwood, Massachusetts 02062.

16. Augustadt, H.W., "Electronic Filter," U.S. Patent 2,106,785, February, 1938.

17. Scott, H.H., "A New Type of Selective Circuit and Some Applications," Proc. IRE, Vol. 6, pp. 226-235, February, 1938.

18. Stanton, L., "Theory and Application of Parallel-T Resonance Capacitance Frequency-Selective Networks," Proc. IRE, Vol. 34, pp. 447-456, July, 1946.

19. Sallen, R.P. and Ken, E.L., "A Practical Method of Designing RC Active Filters," IRE Trans. Circuit Theory, Vol. CT-2, pp. 74-85, March, 1955.

20. Muschy, G.S. and Thelen, W., "Design of Hybrid Integrated-Filter Blocks," IEEE Journal of Solid State Circuits, Vol. SC-5, No. 3, pp. 99-107, June, 1970.

21. Geffe, P.R., "Passive Q Sensitivities of the Twin-T Selective Amplifier," IEEE Trans. Circuit Theory, CT-19, No. 6, pp. 685-686, November, 1972.

22. Gray, P.E. and Searle, C.L., Electronics Principles; Physics, Models and Circuits, Wiley and Sons, 1969.

23. Everitt, W.L., Communication Engineering, McGraw-Hill, 1937.

24. Selected Raman Spectral Data, Report of American Petroleum Institute, Research Project 44, Thermodynamic Research Center, Department of Chemistry, Texas A & M University, College Station, Texas.

25. Wood, R.W., Physical Optics, Macmillan Co., 1936.

26. Sparrow, C.M., "Theory of Imperfect Gratings," The Astrophysical Journal, Vol. 49, pp. 65-95, 1919.

BIOGRAPHICAL SKETCH

Wallace Dorman Kilpatrick was born at Worcester, Massachusetts, on August 31, 1920. He was graduated from North High School in Worcester, Massachusetts; attended Antioch College in Yellow Springs, Ohio; and graduated from Clark University in Worcester, Massachusetts, with the degree of Bachelor of Arts in 1942. He studied Radio Engineering at Harvard University, Cambridge, Massachusetts; Ultra High Frequency Engineering at Massachusetts Institute of Technology, Cambridge, Massachusetts; and graduate Physics at the University of California at Berkeley, California. He was graduated from Florida Atlantic University at Boca Raton, Florida, with the degree of Master of Science in Physics in 1970.

During WWII he was technical officer for airborne and shipborne electronic equipment, including radio and radar, aboard the light carrier CVE White Plains. He was Instructor of Mathematics at Worcester Polytechnic Institute in Worcester, Massachusetts. His experimentation background has been obtained with the Lawrence Radiation Laboratory (both in Berkeley and Livermore, California); with industrial research at Electro-Optical Systems, Inc., Pasadena, California; and with Franklin GNO Corporation, West Palm Beach, Florida.

I certify that I have read this study and that in my opinion it conforms to acceptable standards of scholarly presentation and is fully adequate, in scope and quality, as a dissertation for the degree of Doctor of Philosophy.

David T. Williams

David T. Williams, Chairman
Professor of Aerospace Engineering

I certify that I have read this study and that in my opinion it conforms to acceptable standards of scholarly presentation and is fully adequate, in scope and quality, as a dissertation for the degree of Doctor of Philosophy.

Dennis R. Keefer
Associate Professor of
Aerospace Engineering

I certify that I have read this study and that in my opinion it conforms to acceptable standards of scholarly presentation and is fully adequate, in scope and quality, as a dissertation for the degree of Doctor of Philosophy.

Edward K. Walsh
Associate Professor of
Aerospace Engineering

I certify that I have read this study and that in my opinion it conforms to acceptable standards of scholarly presentation and is fully adequate, in scope and quality, as a dissertation for the degree of Doctor of Philosophy.

Thomas L. Bailey
Professor of Physics

I certify that I have read this study and that in my opinion it conforms to acceptable standards of scholarly presentation and is fully adequate, in scope and quality, as a dissertation for the degree of Doctor of Philosophy.

James W. Dufty
Associate Professor of Physics

This dissertation was submitted to the Graduate Faculty of the College of Engineering and to the Graduate Council, and was accepted as partial fulfillment of the requirements for the degree of Doctor of Philosophy.

June, 1975

Dean, College of Engineering

Dean, Graduate School

UNIVERSITY OF FLORIDA
3 1262 08553 0458